β-importins Tnpo-SR and Cadmus and the small GTPase Ran promote ovarian cyst formation in *Drosophila*

Allison N. Beachum, Taylor D. Hinnant, Anna E. Williams, Amanda M. Powell, and Elizabeth T. Ables*

Department of Biology, East Carolina University, Greenville, NC 27858.

*Correspondence: ablese@ecu.edu; 1001 E. 10th St. Mailstop 551, Greenville, NC 27858; Phone: 252-328-9770; Fax: 252-328-4178

RUNNING TITLE

importins promote cyst formation

KEYWORDS

Oocyte, oogenesis, germline, cyst, germline stem cell

CORRESPONDING AUTHOR:

Elizabeth T. Ables
East Carolina University
Department of Biology
1001 E. 10th St., Mailstop 551
553 Science & Technology Building
Greenville, NC 27858
Office phone: 252-328-9770
e-mail: ablese@ecu.edu

SUMMARY STATEMENT

Ran and two β-importins function independently to promote oocyte selection and cyst development in the *Drosophila* ovary, likely by regulating distinct cargos critical for cell cycle progression.

ABSTRACT

Germ cells undergo mitotic expansion via incomplete cytokinesis, forming cysts of undifferentiated cells that remain interconnected prior to meiotic initiation, through mechanisms that are not well-defined. In somatic cells, an actomyosin contractile network controls cleavage furrow formation and abscission and is spatiotemporally regulated by Ras-related nuclear protein (Ran). Here, we identify Ran and β-importins as critical regulators of cyst development in the *Drosophila* ovary. Depletion of *Ran* or the β-importins *Tnpo-SR* and *cadmus* disrupts oocyte selection and results in egg chambers with variable numbers of germ cells, suggesting abnormal cyst development and cyst fragmentation. We demonstrate that Ran, Tnpo-SR, and Cadmus regulate key cellular processes during cyst formation, including cell cycle dynamics, fusome biogenesis, and ring canal stability, yet do so independently of mitotic spindle assembly. Further, Tnpo-SR and Cadmus control cyclin accumulation and suppress cytokinesis independent of Ran-GTP, suggesting that β-importins sequester protein cargos that normally promote the mitotic-to-meiotic transition. Our data demonstrates that Ran and β-importins are critical for germ cell cyst formation, a role that is likely conserved in other organisms.

48 **INTRODUCTION**

49 Germ cells develop as cysts of undifferentiated cells that remain that remain interconnected
50 during mitotic division (Lu et al., 2017; Matova and Cooley, 2001; Pepling and Lei, 2018). Cysts
51 arise via incomplete cytokinesis, manifested by cleavage furrow arrest and the subsequent
52 formation of stable ring canals that interconnect cells and allow transport of cytoplasm and
53 organelles (de Cuevas et al., 1997; Guertin et al., 2002; Haglund et al., 2011; Pepling and Lei,
54 2018). Cyst formation has been postulated to increase cytoplasmic volume, enhance sensitivity to
55 DNA damage, and ensure robust oocyte development (Chaigne et al., 2020; de Cuevas et al., 1997;
56 Pepling and Lei, 2018; Pepling et al., 1999; Yamashita, 2018). The evolutionary conservation of
57 cyst formation suggests that germ cell interconnectivity is biologically relevant and in support of
58 this, stable intercellular bridges are required for optimal fertility in multiple phyla (Haglund et al.,
59 2011; Lu et al., 2017).

60 The fruit fly, *Drosophila melanogaster*, is an elegant model of germline cyst formation. In
61 adult females, ovaries consist of 16-20 ovarioles, in which oocytes are produced in a linear
62 spatiotemporal arrangement fueled by a tissue-resident stem cell population (Hinnant et al., 2020).
63 Germline stem cells (GSCs) are housed at the anterior of ovarioles within a somatic cell niche
64 (Figure 1A). GSCs divide asymmetrically, giving rise to one daughter that will remain a GSC and
65 a cystoblast which initiates differentiation. Delayed abscission between the GSC and nascent
66 cystoblast keeps the pair connected well into G2 of the subsequent cell cycle (Ables and
67 Drummond-Barbosa, 2013; Eikenes Å et al., 2015; Hinnant et al., 2017; Mathieu et al., 2013;
68 Matias et al., 2015). Following abscission, cystoblasts divide exactly four times with incomplete
69 cytokinesis, creating 16-cell cysts. During and following mitotic division, cleavage furrows
70 between germ cells are modified into stable ring canals, which facilitate organelle transport to and
71 selection of one definitive oocyte within the 16-cell cyst (Grieder et al., 2000; Guertin et al., 2002;
72 Hinnant et al., 2020). The fusome, an unusual cytoplasmic organelle composed of microtubules,
73 endoplasmic reticulum-derived vesicles, and a meshwork of membrane skeleton proteins, traverses
74 the intercellular bridges of GSC/cystoblast pairs and cysts (Hinnant et al., 2020; Ong and Tan,
75 2010; Pepling and Lei, 2018; Röper, 2007; Snapp et al., 2004). The fusome branches as mitotic
76 divisions progress, providing a synchronization hub for cell cycle regulation and cell polarity
77 (Grieder et al., 2000; Hinnant et al., 2020; Lighthouse et al., 2008). These specialized cytological
78 features of germ cells facilitate interconnectivity and are vital to oocyte selection; however, the

79 molecular mechanisms underlying fusome morphogenesis and incomplete cytokinesis are not well
80 understood.

81 In cells that undergo complete cytokinesis, formation of an actomyosin-based contractile
82 network at the equatorial cleavage plane is spatiotemporally regulated and requires a dynamic
83 interplay between the cytoskeleton, the mitotic microtubule-based central spindle, and membrane
84 trafficking (Frémont and Echard, 2018; Haglund et al., 2011; Nguyen and Robinson, 2020; Pollard
85 and O'Shaughnessy, 2019). Central to this process is Ras-related nuclear protein (Ran), a small
86 guanosine triphosphate (GTP)-binding protein implicated in protein transport during mitosis and
87 interphase (Ozugergin and Piekny, 2020; Sazer and Dasso, 2000). Ran partners with α- and β-
88 importins to move protein cargo into the nucleus and promote mitotic spindle assembly (Cautain
89 et al., 2015; Okada et al., 2008). Ran also regulates cell polarization and contractile protein
90 localization during cleavage furrow ingression (Beaudet et al., 2017; Silverman-Gavrila et al.,
91 2008). Chromatin-associated Ran-GTP may help recruit and organize essential proteins at the
92 cortex, thereby ensuring the robustness of cytokinesis (Nguyen and Robinson, 2020). The
93 biological relevance of importins or Ran to germline cyst formation has not been established.

94 Here, we identify Ran and β-importins as novel regulators of GSC maintenance and germ
95 cell cyst formation in the *Drosophila* ovary. We show that Ran and β-importins Tnpo-SR and
96 Cadmus (Cdm) control cyst formation by regulating key cellular processes, including cell cycle
97 dynamics, fusome biogenesis, and ring canal stability. Ran function depends on its active, GTP-
98 bound state, as expression of a dominant-negative *Ran* mutant recapitulates *Ran* loss-of-function.
99 *Ran*, *Tnpo-SR*, and *cdm* are not essential for mitotic spindle formation in undifferentiated germ
100 cells. Moreover, knock-down of *Tnpo-SR* or *cdm* does not completely phenocopy loss of *Ran*,
101 suggesting that β-importins control cell cycle progression and suppress cytokinesis independent of
102 Ran activity. Given the conservation of germline cyst formation across phyla, our data suggest that
103 Ran and specific β-importins may play similar roles in other organisms.

104

105 **RESULTS**

106 ***RNAi screen reveals that β-importins and Ran are essential for germ cell development.***

107 We previously identified *Transportin-Serine/Arginine rich* (*Tnpo-SR*) in a genetic mosaic
108 screen for genes controlling GSC self-renewal (Ables et al., 2016). *Tnpo-SR*, homologous to
109 mammalian *TNPO3*, encodes a β-importin (Allemand et al., 2002; Lai et al., 2001). To determine

110 whether *Tnpo-SR* loss-of-function phenotypes reflect a general role for importins in germ cell
111 mitoses, we performed a secondary reverse genetic screen using germline-enhanced RNA
112 interference (RNAi) to knock-down expression of nine *Drosophila* importins and the small
113 GTPase *Ran* specifically in germ cells (Figure 1B-E) (Ni et al., 2011; Rørth, 1998; Van Doren et
114 al., 1998). Ovarioles were quantified for the presence of germ cells based on the unique nuclear
115 morphology of nurse cells and oocytes (Figure 1B). Most of the RNAi lines produced ovarioles
116 with seven to eight egg chambers, similar to driver-only controls (Figure 1B,E). In contrast, three
117 RNAi lines produced completely agametic ovaries, defined by the absence of egg chambers
118 (Figure 1C,E). RNAi line *Tnpo/CG8219*^{HMJ23009} carries a short hairpin that recognizes both *Tnpo*
119 and the related paralog *CG8219*. Since two other RNAi lines specific for *Tnpo* did not display
120 germ cell phenotypes, we speculate that Tnpo and CG8219 may compensate for each other, as they
121 share 80% amino acid similarity. Only one RNAi line for the β-importin *moleskin* (*msk*^{HMS00020})
122 displayed an agametic phenotype, making it difficult to conclude whether the RNAi accurately
123 reflects a role in germ cell development. More intriguingly, four RNAi lines corresponding to *Ran*
124 and the β-importins *Tnpo-SR*, *cadmus* (*cdm*), and *Fs(2)Ket* (also called *Ketel*) exhibited a partial
125 agametic phenotype (Figure 1D-E). Some ovarioles lacked germ cells, while other ovarioles
126 contained germ cells in unusual egg chamber morphologies (Figure 1D). Cdm and Tnpo-SR are
127 paralogs, sharing 42% amino acid similarity, while Ketel is less conserved. These results
128 demonstrate that Ran and β-importins are necessary for proper oocyte development and may have
129 distinct yet overlapping functions in the germline.
130

131 ***Ran, Tnpo-SR, Ketel, and cdm are necessary to establish GSCs.***

132 Since GSCs give rise to all germ cells, we hypothesized that agametic ovaries resulting
133 from *Ran* and *β-importin* knock-down could arise from a failure to establish or maintain GSCs. To
134 test this, we collected ovaries from control and germ cell *Ran* or *β-importin* RNAi knock-down
135 females at successive days after eclosion and quantified the number of GSCs per germarium. GSCs
136 and their progeny can be easily identified by immunolabeling of Hts, a fusome-resident protein in
137 germ cells, and LaminC (LamC), a nuclear envelope protein highly expressed in cap cells (the
138 major cellular component of the GSC niche) (Ables and Drummond-Barbosa, 2013). While
139 fusomes are present in GSCs and their dividing daughters, only GSCs possess an anteriorly
140 localized fusome juxtaposed to the cap cells (de Cuevas and Spradling, 1998; Lin et al., 1994).

141 Driver control ovaries averaged 2.8 GSCs per germarium just after eclosion, and consistent with
142 previous studies, the average decreased slightly over time as females aged (Supp. Figure 1A,C)
143 (Pan et al., 2007). All four RNAi lines giving a partial agametic phenotype upon germline-specific
144 knock-down had significantly less GSCs per germarium at three days after eclosion (Supp. Figure
145 1B-C). Fewer GSCs in early adulthood suggests that *Ran*, *Tnpo-SR*, and *cdm* are required for GSC
146 establishment during larval/pupal stages or during the proliferative surge in GSCs following the
147 female's first mating (Ameku and Niwa, 2016; Van Doren et al., 1998). The number of GSCs per
148 germarium continued to decline with age following knock-down of *Ran*, *Tnpo-SR*, and *cdm* (Supp.
149 Figure 1C).

150 To test whether Ran or β-importins are also required for GSC maintenance, we used a
151 conditional knock-out approach to specifically abrogate *Tnpo-SR* in adult GSCs and quantified the
152 number of GSCs remaining in the tissue over time. The *Flippase* (*FLP*)/*FLP Recognition Target*
153 (*FRT*) genetic mosaic lineage-tracing system allows for the generation of clonal populations of
154 homozygous mutant cells in otherwise heterozygous animals (Laws and Drummond-Barbosa,
155 2015; Xu and Rubin, 1993). We used two strong loss-of-function transposon insertion alleles of
156 *Tnpo-SR* (*Tnpo-SR*^{KG04870} and *Tnpo-SR*^{LL05552}) carrying *FRT* sites to generate germline mutant
157 mosaic germaria (Supp. Figure 1D-F). To quantify GSC loss, we measured the percentage of total
158 germaria harboring a mutant (GFP-negative) GSC. Mock mosaic germaria were used as controls,
159 as GFP-negative GSCs can be produced even though all cells are genotypically wild-type (Supp.
160 Figure 1D). GFP-negative GSC clones were generated at equivalent rates in control, *Tnpo-*
161 *SR*^{KG04870}, and *Tnpo-SR*^{LL05552} mosaic germaria at four days after clone induction (Supp. Figure
162 1F). In contrast to mock controls, *Tnpo-SR*^{KG04870} and *Tnpo-SR*^{LL05552} germline mutant mosaic
163 germaria rapidly lost marked GSCs over time (Supp. Figure 1E,F), indicating that *Tnpo-SR* is cell-
164 autonomously required for GSC self-renewal. *Tnpo-SR* mutant GSCs likely adhere to cap cells as
165 well as adjacent wild-type GSCs, as they express equivalent levels of the adhesion protein E-
166 cadherin (Supp. Figure 1G,G'). Loss of *Tnpo-SR* appears to uncouple cell growth and cell division,
167 as *Tnpo-SR* mutant GSCs grow larger than adjacent wild-type GSCs (Supp. Figure 1G,G'),
168 reminiscent of *Cdk2* or *CycE* null GSCs (Ables and Drummond-Barbosa, 2013). Taken together
169 with the RNAi data, these results suggest prominent roles for *Ran*, *Tnpo-SR,* and *cdm* in GSC
170 maintenance.
171

172 ***Loss-of-function mutations in Ran and β-importins alter the number of germ cells per egg***
173 ***chamber.***

174 The intriguing agametic phenotype resulting from knock-down of *Ran*, *cdm*, *Tnpo-SR*, and
175 *Ketel* prompted us to take a closer look at egg chamber morphology. Egg chambers develop in a
176 stereotypical fashion, where germline cysts are encapsulated by a monolayer of follicle cells as
177 cysts move posteriorly out of the germarium (Figure 1A). To visualize germline and follicle cells,
178 we combined anti-Hts antibodies (which detect Hts at the plasma membrane in follicle cells) with
179 anti-Hts-RC antibodies, which are specific for a cleavage product of the Hts polyprotein that
180 localizes to ring canals (Petrella et al., 2007; Robinson et al., 1994). Driver control egg chambers
181 had 16 germ cells connected by 15 ring canals (Figure 2A,D). Knock-down of *Ran*, *cdm*, or *Tnpo-*
182 *SR*, however, resulted in significantly less egg chambers with 16 germ cells (Figure 2B-D).
183 Depletion of *Ketel* did not significantly impact egg chamber morphology (Figure 2D).

184 Germ cell cysts normally divide synchronously four times, following a 2^n pattern, to
185 produce cysts with 16 cells (King, 1970). To determine whether extra germ cells in *Ran*, *cdm*, and
186 *Tnpo-SR* depleted ovarioles arose by alterations in the number of mitotic divisions, we quantified
187 the number of germ cells per cyst (Figure 2E). In both control and *Ketel* RNAi ovaries, egg
188 chambers rarely contained more than 16 cells (Figure 2D,F); in these rare instances, egg chambers
189 invariably contained 32 cells (Figure 2E). In contrast, knock-down of *Ran*, *cdm,* or *Tnpo-SR*
190 produced egg chambers with variable numbers of germ cells, ranging anywhere from one to 49
191 cells per cyst (Figure 2E). While some egg chambers housed germ cells on the order of 2^n, a
192 substantial number deviated from this pattern (Table 1). Ggerm cell numbers in adjacent chambers
193 in RNAi-depleted egg chambers did not add up to 8, 16 or 32 cells, arguing that encapsulation
194 defects alone are not the source of the unusual germ cell number phenotype. Some egg chambers
195 with 32 or more cells had oocytes with five ring canals, suggesting that some abnormal egg
196 chambers arose by an extra mitotic division. Other egg chambers, however, likely arose because
197 of other cellular defects. Moreover, a small percentage of *Tnpo-SR* and *cdm* RNAi knock-down
198 ovarioles (13.3% and 17.4% of the total number of ovarioles, respectively) contained germline
199 tumors, in which a few abnormally-shaped egg chambers with a seemingly normal follicle cell
200 monolayer surrounded mitotically-active germ cells with underdeveloped fusomes (Figure 2G-H;
201 Supp. Figure 2A-C'). In *Tnpo-SR* RNAi ovarioles, undifferentiated germ cells were found
202 encapsulated with more-developed germ cells (Supp. Figure 2A). Germline tumors contained cells

203 with short or unbranched fusomes, resembling those of 2-cell cysts, and immature ring canals that
204 frequently appeared as dot-like structures rather than rings (Supp. Figure 2A-B). These structures
205 are reminiscent of the abscission site in the cytokinetic furrow separating GSC/cystoblast pairs
206 (Supp. Figure 1I-K), suggesting that some tumors arose because of improper abscission events in
207 2-cell and/or 4-cell cysts. Immunostaining for Sex-lethal (Sxl), which is enriched in GSCs and
208 cystoblasts in the anterior-most region of the germarium (Supp. Figure 2D-D') (Chau et al., 2009),
209 confirmed that *Tnpo-SR* RNAi germ cells have not completed differentiation, as Sxl was expressed
210 at similar levels in cells throughout the germarium (Supp. Figure 2E-E'). We conclude that Ran,
211 Tnpo-SR, and Cdm impact the synchrony and number of cyst divisions.
212
213 ***Ran, Tnpo-SR, and cdm are required for oocyte specification.***
214 During germ cell mitotic divisions, three to four cyst cells initiate meiosis by assembling
215 the synaptonemal complex; however, only one of these cells is maintained as the oocyte (Hughes
216 et al., 2018). Since depletion of *Ran*, *Tnpo-SR*, or *cdm* altered the number of germ cells per cyst,
217 we hypothesized that oocyte selection was also affected. We analyzed the first three egg chambers
218 outside of the germarium, where the oocyte-specific proteins Orb (Figure 3A) and Bicaudal D
219 (BicD) (Figure 3D) had clearly accumulated in one posterior cyst cell in driver control egg
220 chambers. In contrast, knock-down of *Ran*, *Tnpo-SR*, or *cdm* resulted in egg chambers lacking
221 either Orb ($Ran^{GL01341}$, $cdm^{HMS02846}$, and $Tnpo\text{-}SR^{V22}$) or BicD expression ($Tnpo\text{-}SR^{V22}$) (Figure 3B-
222 C, E-F). Moreover, many *Ran*, *Tnpo-SR*, and *cdm* loss-of-function egg chambers lacked a cell with
223 a condensed nucleus or karyosome, a clear indicator of oocyte specification (Figure 3B,E,F). Since
224 knock-down of *Ran*, *Tnpo-SR*, and *cdm* can alter the number of cells per cyst, we quantified only
225 egg chambers with 16 cyst cells (Figure 3G). Although the majority of $nos\text{-}Gal4{>}Ran^{GL01341}$ and
226 $nos\text{-}Gal4{>}cdm^{HMS02846}$ successfully specified a single oocyte, 34% of $nos\text{-}Gal4{>}Tnpo\text{-}SR^{V22}$ egg
227 chambers contained only nurse cells (Figure 3G). These data suggest that loss of oocyte identity
228 is a secondary effect of incorrect mitotic divisions in the absence of *Ran* and *cdm*, but that *Tnpo-*
229 *SR* may play independent roles in oocyte specification. We therefore immunostained for Orb in
230 *Tnpo-SR* mutant mosaic germaria and counted the number of 16-cell cysts in the germarium with
231 at least one Orb-positive cell. $Tnpo\text{-}SR^{KG04870}$ mutant cysts located posterior to wild-type cysts (and
232 thus at a more advanced stage of development) failed to up-regulate Orb expression to similar
233 levels as adjacent wild-type cysts (Figure 3H-I). Moreover, a core component of the synaptonemal

234 complex, C(3)G, which is normally present as early as the 4-cell cyst stage, did not accumulate in
235 *Tnpo-SR*^{KG04870} mutant 8-cell or 16-cell cysts to equivalent levels as adjacent wild-type cysts
236 (Figure 3J-K). Together with the RNAi data, this suggests that *Tnpo-SR* is specifically required for
237 oocyte specification.
238
239 ***GSC establishment, cyst formation, and oocyte selection require active Ran-GTP.***
240 Since Ran and β-importins work together to drive nucleocytoplasmic transport in other
241 systems (Chang and Hsia, 2020; Nguyen and Robinson, 2020; Ozugergin and Piekny, 2020), we
242 expected that depletion of *Ran* would phenocopy loss of either *Tnpo-SR* or *cdm*. Our data, however,
243 revealed key differences between the loss-of-function phenotypes, suggesting that β-importins
244 might have roles in germ cell cyst formation independent of Ran, or cellular functions other than
245 cytoplasmic-to-nuclear trafficking.
246 To test these possibilities, we first analyzed the subcellular distribution of Ran in
247 mitotically dividing germ cells. We took advantage of a previously characterized transgene in
248 which the germline-specific *UASp* promoter drives an N-terminal hemagglutinin (HA)-tagged Ran
249 coding region (*UASp-Ran*^{HA}) (Cesario and McKim, 2011). Using *nos-Gal4* to drive *UASp-Ran*^{HA}
250 in germ cells, we then localized Ran using anti-HA antibodies in comparison to mitotic spindles
251 (labeled with α-tubulin), fusomes, and chromosomes (Figure 4A-A'). Unlike neuroblasts, in which
252 Ran-HA is nuclearly localized during interphase and overlaps with the mitotic spindle during
253 mitosis (Cesario and McKim, 2011), we did not observe strong nuclear localization of Ran-HA in
254 GSCs or dividing germ cells (Figure 4A-A'). Ran-HA was evenly distributed, or slightly higher in
255 the cytoplasm than in nuclei, of interphase and mitotically-dividing cells. Consistent with
256 neuroblasts and embryonic cells (Cesario and McKim, 2011; Trieselmann and Wilde, 2002), we
257 did not observe Ran on chromosomes (Figure 4A'). Ran-HA expression was higher in some cysts
258 than others, likely due to minor variations in driver strength. Moreover, and in contrast to the
259 meiotic spindles in late stage egg chambers (Cesario and McKim, 2011), we did not observe strong
260 accumulation of Ran-HA surrounding mitotic spindles (Figure 4A-A'). Lack of strong nuclear
261 localization or accumulation at spindles argues against roles for Ran in cytoplasmic-to-nuclear
262 trafficking or mitotic spindle formation in dividing germ cells.
263 We next asked whether active Ran-GTP is required for GSC establishment and cyst
264 formation. Like other small GTP-binding proteins, Ran cycles between active (GTP-bound) and

265 inactive (GDP-bound) states (Ozugergin and Piekny, 2020). Ran-GTP dissociates importin-bound
266 cargo, increasing the amount of free importin available to bind cargo. We over-expressed two
267 transgenes carrying mutated forms of Ran in germ cells under the control of *nos-Gal4*. The first
268 transgene, *UASp-Ran*^{T24N}, carries an amino acid substitution that locks Ran into a GDP-bound state
269 and inhibits cargo loading (Cesario and McKim, 2011; Drutovic et al., 2020). Mutant flies were
270 compared to flies expressing wild-type *UASp-Ran*^{HA}. We expected that constitutively expressing
271 Ran-GDP would titrate out the amount of active Ran, thus mimicking *Ran* loss-of-function.
272 Indeed, over-expression of *UASp-Ran*^{T24N} resulted in a partial agametic phenotype (Figure 4B,F),
273 and the average number of GSCs per germarium was substantially reduced as compared to age-
274 matched *nos-Gal4>UASp-Ran*^{HA} controls (Figure 4G). Over-expression of dominant negative
275 *Ran*^{T24N} also altered the number of germ cells per cyst (Figure 4C,J) and, similar to knock-down
276 of *Ran* via RNAi (Figure 2E), the number of germ cells did not always follow a 2^n pattern (Figure
277 4I, Table 1). Over-expression of *Ran*^{T24N} also impaired oocyte selection, as 12-24% of egg
278 chambers with 16 germ cells lacked an Orb-positive cell (Figure 4J). These phenotypes are
279 consistent with depletion of *Ran* via RNAi and likely contribute to the female sterility phenotype
280 noted in prior studies (Cesario and McKim, 2011).

281 We then used a second transgene, *UASp-Ran*^{Q69L}, to over-express a constitutively active
282 form of Ran locked in a hydrolysis-resistant GTP-bound state (Cesario and McKim, 2011).
283 Intriguingly, excess Ran-GTP in germ cells did not result in severe germline defects (Figure 4E-
284 F). The average number of GSCs per germarium was slightly reduced in *nos-Gal4>UASp-Ran*^{Q69L}
285 ovarioles (Figure 4G) and a few egg chambers had an incorrect number of cells (Figure 4H-I), but
286 defects were not as severe or penetrant as either the *Ran* RNAi or Ran-GDP-locked mutants. Since
287 we did not observe a clear Ran intracellular concentration gradient or accumulation of Ran at
288 mitotic spindles, these results suggest that Ran-GTP levels are already in excess in mitotically-
289 active germ cells, perhaps to facilitate timely mitotic divisions.

290

291 ***Ran-GTP, Tnpo-SR, and cdm are dispensable for mitotic spindle formation in dividing cysts.***

292 One well-characterized function of Ran and β-importins is the regulation of spindle
293 assembly (Forbes et al., 2015; Kosyna and Depping, 2018). Spindle orientation is critical for GSC
294 maintenance, and mitotic spindle remnants accumulate in fusomes as cysts divide (Cheng et al.,
295 2008; Deng and Lin, 1997; Grieder et al., 2000; Máthé et al., 2003). We hypothesized that primary

296 defects in spindle formation could underlie the defective cyst division in our Ran-GTP and
297 importin-depleted models. Using immunostaining for α-Tubulin, we confirmed that mitotic
298 spindles in dividing cysts are anchored to the fusome, oriented perpendicularly (Figure 5A)
299 (Megraw and Kaufman, 2000; Storto and King, 1989). Surprisingly, in *cdm*-depleted (Figure 5B)
300 or *Tnpo-SR*-depleted (Figure 5C) germ cells, similar-sized spindles formed and were appropriately
301 anchored and oriented with respect to fusomes. Similarly, we were unable to find defects in spindle
302 formation or orientation in *nosGal4>UAS-Ran*^{T24N} germ cells (Figure 5D). These data demonstrate
303 that mitotic spindles can form even when Ran-GTP is depleted, suggesting that very low levels of
304 active Ran are sufficient to maintain germ cell mitoses.
305
306 ***Tnpo-SR and cdm, but not Ran-GTP, are required for fusome biogenesis and maturation.***
307 The fusome extends through ring canals during incomplete cytokinesis, forming an
308 extensive tubular network (Lighthouse et al., 2008; Röper, 2007; Snapp et al., 2004). The balance
309 of cytoskeleton to vesicular-like structures in the fusome changes over the course of the mitotic
310 divisions, as the cytoskeletal core (which can be visualized with anti-Hts antibodies; Figure 5E) is
311 prominent in GSC and cystoblast fusomes, but eventually degrades as cysts exit the germarium
312 (Röper, 2007). Loss of *Hts* alters the number of germ cells per cyst (Yue and Spradling, 1992).
313 Since knock-down of *Ran* or the β-importins also altered the number of germ cells per cyst, we
314 hypothesized that abnormal fusome morphogenesis might abrogate cyst formation. Using Hts
315 immunostaining as an indicator of fusome morphology, we observed that when *cdm* (Figure 5F)
316 or *Tnpo-SR* (Figure 5G and Supp. Figure S2) were depleted, germ cells formed long, thin fusomes
317 with irregular branching, particularly in cysts in the middle to posterior third of germaria. Fusomes
318 in *Tnpo-SR*- and *cdm*-depleted germ cells often had thread-like sections separated by thicker
319 sections, consistent with weak points in the cytoskeletal structure (see arrowheads in Figure 5F-
320 G). Irregular fusomes were also observed in *Tnpo-SR*-depleted GSC/cystoblast pairs, where new
321 fusome material builds from the cystoblast to the GSC (Supp. Figure 1 I-J) (de Cuevas and
322 Spradling, 1998). Importantly, we did not observe fusomes connecting GSCs to other cyst cells in
323 stem-cysts, as was reported for germ cells in which the chromosomal passenger complex, which
324 regulates abscission timing in GSCs, is abrogated (Mathieu and Huynh, 2017). We also did not
325 observe GSCs or cysts with asynchronous mitoses (Supp. Figure S1L-M), as we would predict if
326 fusomes did not maintain some degree of connectivity between cells. We conclude that the

327 irregular fusome branching patterns in *Tnpo-SR*- and *cdm*-depleted germ cells likely result from
328 impaired fusome maintenance or remodeling.

329 To further investigate how the importins regulate fusome morphogenesis, we recombined
330 the *Tnpo-SR*^{V22} RNAi transgene with two reporter transgenes in which the coding regions of
331 fusome-resident proteins were fluorescently tagged. *Scribble* (*scrib*) encodes a scaffolding protein
332 that regulates vesicle trafficking and is expressed at the cell cortex and in immature fusomes of
333 GSCs and dividing cysts (Figure 5I) (Lighthouse et al., 2008). By the third mitotic division, *Scrib-*
334 *GFP* is largely absent from wild-type fusomes and does not co-localize with Hts in 16-cell cysts.
335 In *Tnpo-SR*-depleted germ cells, however, *Scrib-GFP* was prominently expressed in the long, thin
336 fusomes of germ cells in the posterior of germaria (Figure 5J). Conversely, Reticulon-like1 (Rtnl1)
337 is an endoplasmic reticulum-resident protein that is expressed in low levels in immature fusomes
338 (Figure 5K) (Röper, 2007). *Rtnl1-GFP* becomes enriched in mature fusomes coincident with cyst
339 division and inversely correlated with Hts expression, reaching peak concentration in fusomes
340 after the final mitotic division (Figure 5K). When *Tnpo-SR* is knocked down in germ cells, *Rtnl1-*
341 *GFP* and Hts co-localize in fusomes throughout the posterior end of the germarium (Figure 5L).
342 These data suggest that in the absence of β-importins, cytoskeletal components of the fusome fail
343 to degrade properly, maintaining the fusome in an immature state that is weakly connected between
344 cyst cells. Intriguingly, fusome shape and branching in cysts over-expressing the dominant
345 negative *Ran*^{T24N} mutant (Figure 5D) were indistinguishable from wild-type cysts, suggesting that
346 Cdm and Tnpo-SR regulate fusome morphogenesis independently of Ran-GTP.

347

348 ***Tnpo-SR and cdm promote cyst formation by suppressing cytokinesis.***

349 Knock-down of *Tnpo-SR* or *cdm* produced egg chambers variable numbers of germ cells;
350 however, it remained unclear to us exactly how such egg chambers could arise. Key observations
351 came by closely examining the morphology of *Tnpo-SR* mutant cysts surrounded by wild-type
352 cysts in mutant mosaic germaria. While knock-down of *Tnpo-SR* by RNAi led to >16 germ cells
353 per egg chamber, we only rarely found examples of *Tnpo-SR*^{KG04870} or *Tnpo-SR*^{LL05552} mutant egg
354 chambers with more than 16 mutant germ cells. We did find, however, compound egg chambers
355 in which a *Tnpo-SR* mutant cyst was encapsulated together with wild-type cysts (Supp. Figure
356 S3A). We occasionally identified mitotically-dividing *Tnpo-SR*^{KG04870} and *Tnpo-SR*^{LL05552} mutant
357 germ cells in mosaic egg chambers outside of the germarium, which never occurs in wild-type

358 germ cells (Supp. Figure S3B). We also frequently found clusters of single *Tnpo-SR* mutant germ
359 cells at the posterior of germaria (Supp. Figure S3C), suggesting that some cyst defects in *Tnpo-*
360 *SR* mutant and RNAi-knock-down ovarioles could arise by fragmentation of cysts into single germ
361 cells. In the *Tnpo-SR* RNAi model, where all germ cells lack appropriate Tnpo-SR levels,
362 fragmented cysts would likely be encapsulated along with adjacent cysts, thus yielding irregular
363 (i.e., not 2^n) numbers of germ cells per cyst. In support of this idea, we observed many examples
364 of mutant mosaic germaria in which *Tnpo-SR*^{KG04870} mutant cells with dot-like fusomes were
365 adjacent to one another with fusomes aligned along the same plane, as if they were connected
366 (Supp. Figure S3D). Immunostaining with anti-pTyr antibodies to visualize ring canals highlighted
367 *Tnpo-SR*^{KG04870} mutant cysts where ring canal components accumulated on adjacent cyst cells,
368 separated by a very thin line of GFP-positive cytoplasm (Figure 6A and Supp. Figure S3E),
369 suggesting that cells have physically separated from each other after clone induction. Moreover,
370 *Tnpo-SR*^{KG04870} mutant germ cells failed to accumulate proper levels of the cell adhesion protein
371 E-cadherin between germ cells, as occurs in adjacent wild-type 16-cell cysts following the final
372 mitotic division and prior to follicle cell encapsulation (Figure 6B) (Fichelson et al., 2010).
373 These data raised the possibility that in the absence of *Tnpo-SR*, cysts which normally form
374 via incomplete cytokinesis fail to stay connected by intercellular bridges, and instead break apart
375 at unstable ring canals. Initially, this seemed unlikely, as our first analyses of *Ran*, *cdm*, and *Tnpo-*
376 *SR* RNAi and *Ran* dominant-negative germ cells focused on egg chambers outside of the
377 germarium, where ring canals containing Hts-RC (a constituent protein of mature ring canals) were
378 easily detected (Figure 2). Moreover, the number of ring canals scaled to the number of germ cells,
379 suggesting that ring canals formed at successive divisions. Spatiotemporal comparison of ring
380 canal formation, however, demonstrated that while Hts-RC is expressed in germ cells from *nos-*
381 *Gal4>Tnpo-SR*^{V22} ovarioles, its accumulation at ring canals is drastically delayed, such that protein
382 levels are much lower than in age-matched wild-type cysts (compare Figure 6C and D). Similarly,
383 anti-pTyr antibodies are typically the first molecular indicator of mature ring canals (Figure 6E).
384 In the germ cells depleted of *cdm* (Figure 6F) or *Tnpo-SR* (Figure 6G), pTyr antibodies failed to
385 accumulate to wild-type levels in 16-cell cysts. In contrast, both Hts-RC and pTyr accumulated at
386 well-defined ring canals when the dominant negative *Ran*^{T24N} mutant was expressed in germ cells
387 (Figure 6H). These data support the model that Tnpo-SR and Cdm, but not Ran-GTP, function to
388 stabilize germ cell intercellular bridges, maintaining proper cyst formation (Figure 6M).

389 We then performed immunostaining for Anillin, an actin/myosin-binding protein
390 previously demonstrated as an importin cargo (Beaudet et al., 2017; Beaudet et al., 2020; Chen et
391 al., 2015; Piekny and Maddox, 2010; Silverman-Gavrila et al., 2008). Anillin localization in ring
392 canals begins at the third mitotic division (Figure 6I) (Goldbach et al., 2010). In *Tnpo-SR*-depleted
393 germ cells, we observed Anillin deposition within the intercellular bridge, rather than on
394 surrounding rings (Figure 6J). In contrast, Anillin localizes properly to the ring canals in Ran^{T24N}
395 mutants (Figure 6K) and occasionally co-localized with the fusome (Figure 6L), supporting the
396 model that Tnpo-SR suppresses cytokinesis in dividing cysts independently of Ran-GTP.
397 Intriguingly, over-expression of a GFP-tagged Anillin in which a nuclear localization signal has
398 been mutated did not alter Anillin localization in abscising GSC/CB pairs (Supp. Figure 4A-B) or
399 at ring canals (Supp. Figure 4C-D), and did not change the number of germ cells per cyst. Although
400 we cannot exclude the possibility that Tnpo-SR may bind Anillin at another protein domain, we
401 speculate that Tnpo-SR indirectly regulates Anillin by binding other cargo proteins that impact
402 Anillin localization.
403
404 ***Ectopic CycA accumulates in Tnpo-SR- and cdm-depleted germ cells.***
405 The cell cycle is tightly regulated to coordinate cyst formation. For example, loss of
406 function of the mitotic cyclin CycB produces cysts with eight cells, while over-expression of CycA
407 or CycE produces cysts with 32 cells (Lilly et al., 2000; Mathieu et al., 2013; Morris et al., 2005;
408 Ohlmeyer and Schüpbach, 2003). CycA and CycB accumulate at the fusome and phosphorylation
409 of CycB by AuroraB Kinase promotes abscission between GSC/cystoblast pairs (Lilly et al., 2000;
410 Mathieu et al., 2013). Given the phenotypic parallels, we hypothesized that Tnpo-SR and Cdm
411 might regulate cyclin dynamics in dividing germ cells. We confirmed that CycA accumulates at
412 the fusome in ~10% of mitotically dividing cysts, but never associates with the fusome of 16-cell
413 cysts in wild-type tissue (Figure 7A,F). *Ran* depletion in *nos-Gal4>*$Ran^{GL01341}$ germaria did not
414 alter CycA kinetics (Figure 7B,F). In contrast, nearly 40% of mitotically-dividing cysts in *Tnpo-*
415 *SR* and *cdm*-depleted germ cells expressed CycA; moreover, CycA expression was observed in the
416 fusomes of 16-cell cysts at an equivalent rate as dividing cysts, suggesting that germ cells remain
417 mitotic (Figure 7C-D,F).
418 As the highest peak of CycB expression occurs following CycA degradation (Morris et al.,
419 2005), we then asked whether CycB regulation was likewise impacted by loss of the β-importins.

420 We utilized the *Drosophila* Fluorescence Ubiquitin-based Cell Cycle Indicator system (Fly-
421 FUCCI) (Zielke et al., 2014) to ask whether CycB expression was altered in the absence of *Tnpo-*
422 *SR*. Importantly, we used a version of the *UASp-CycB-RFP* transgene that includes a canonical
423 nuclear localization sequence (Hinnant et al., 2017; Zielke et al., 2014). When *Tnpo-SR* was
424 depleted, the *UASp-CycB-RFP* localized to germ cell nuclei; however, significantly fewer
425 mitotically dividing cysts expressed CycB as compared to wild-type controls (Figure 7E,G). Taken
426 together, these data suggest that *Tnpo-SR*, and likely *cdm*, promote proper cyclin dynamics in germ
427 cells, maintaining cysts in the mitotic expansion phase and facilitating coordination between cyst
428 division and fusome morphogenesis.
429

430 **DISCUSSION**

431 During germline cyst formation, cell cycle transitions are precisely controlled to promote
432 mitotic divisions and block cellular abscission. Our study adds new details to our understanding
433 of the molecular regulation of germ cell mitotic expansion, identifying previously undescribed
434 roles for β-importins and the small GTPase Ran in mitotic cell cycle exit during cyst formation.
435 Remarkably, we do not detect a clear cytoplasmic-to-nuclear gradient of Ran protein localization
436 in germ cell nuclei. Nor do we find defects in mitotic spindle assembly, cell size, or DNA
437 condensation in the absence of β-importins or activated Ran. Instead, our data suggest that
438 importins and Ran-GTP promote mitotic exit by distinct, yet complimentary mechanisms. We
439 propose the model that Ran-GTP drives germ cell mitoses by mobilizing cell cycle factors,
440 functioning together with the β-importins Tnpo-SR and Cdm to facilitate transport of cell cycle
441 factors from the fusome to other parts of the cell. We propose that independent of Ran, Tnpo-SR
442 and Cdm sequester cell cycle regulators like CycA and Anillin, titrating the levels of protein
443 accessible to Ran-GTP, counterbalancing mitotic progression. Thus, in the absence of Tnpo-SR or
444 Cdm, CycA levels accumulate, causing germ cells to continue in a proliferative state and impairing
445 fusome stability, ring canal maturation, and oocyte terminal differentiation.
446

447 ***Importins may exhibit non-redundant functions in the Drosophila germline.***

448 The *Drosophila* genome encodes 15 importin proteins, including four α-importins, which
449 function as adaptor proteins linking cargo with nuclear localization signals to β-importins (Kimura
450 and Imamoto, 2014). Although several α-importins have been implicated in oogenesis prior to our

451 study (Geles and Adam, 2001; Mason et al., 2002; Máthé et al., 2000), our study is the first to
452 identify specific roles for β-importins in mitotic expansion. Our data generally support the
453 hypothesis that specific importins regulate distinct aspects of germ cell development (Hogarth et
454 al., 2005; Loveland et al., 2015; Mihalas et al., 2015). We cannot exclude the possibility, however,
455 that RNAi was not sufficient to completely inhibit importin function. For example, Ketel localizes
456 at the nuclear envelope in early embryos and dividing germ cells (data not shown) (Lippai et al.,
457 2000; Tirián et al., 2000; Trieselmann and Wilde, 2002; Villányi et al., 2008), yet we did not
458 observe germ cell mitotic defects in *Ketel*-depleted germ cells. Future studies will need to employ
459 other loss-of-function approaches to test the roles of Ketel and other β-importins more thoroughly.
460 The repertoire of cargo carried by a β-importin determines its role in biological processes
461 and its redundancy with other importins (Kimura and Imamoto, 2014). Although the full extent of
462 protein-protein interactions mediated by Tnpo-SR remains unknown, structural studies indicate
463 that TNPO3 binds proteins involved in chromatin organization, mRNA and protein modification,
464 cell cycle control, and cell-cell communication (Kimura et al., 2017; Maertens et al., 2014). Tnpo-
465 SR is also likely to bind a broad range of cargo proteins, including SR-rich RNA binding proteins.
466 Indeed, Tnpo-SR physically interacts with several proteins essential for mRNA splicing and
467 transport (Allemand et al., 2002). Given that SR-rich proteins facilitate diverse RNA processing
468 events, there are many potential Tnpo-SR cargo proteins that could influence cyst formation and
469 GSC self-renewal, which are heavily influenced by translational control (Bradley et al., 2015;
470 Teixeira and Lehmann, 2019). Our future studies will seek to identify Tnpo-SR and Cdm-
471 interacting proteins, which should provide additional mechanistic details regarding how importins
472 regulate germ cell mitotic expansion.
473
474 ***The number of cyst divisions is regulated by Ran-GTP and β-importins.***
475 Two major cell fate transitions accompany the development of *Drosophila* oocytes: stem
476 cell to differentiating progenitor (the cystoblast), and progenitor to differentiated fate. These
477 transitions are accompanied by changes in cell cycle control, including a dramatic switch from
478 mitotic expansion to meiosis as terminal differentiation proceeds. How such cell cycle transitions
479 are accomplished is of broad scientific interest, both in the germline and in somatic cells, where
480 exit from the cell cycle accompanies differentiation (Liu et al., 2019). Intriguingly, both cell fate
481 transitions employ common cell cycle regulatory factors, such as cyclins, Cdks, and ubiquitin

482 ligases, suggesting that these are largely repurposed or differentially regulated from GSCs to
483 differentiating cyst cells. Precise spatiotemporal control over cell cycle regulators must therefore
484 underlie the transition to the oocyte fate. In support of this, the mitotic cyclin CycA is clearly
485 critical to support differentiation. Failure to degrade CycA leads to self-renewal failure in GSCs,
486 and extra mitotic divisions and loss of oocyte identity in cyst cells (Chen et al., 2009; Ji et al.,
487 2017; Lilly et al., 2000; Morris et al., 2005; Ohlmeyer and Schüpbach, 2003; Sugimura and Lilly,
488 2006). Moreover, the deubiquitinase encoded by *bag of marbles* (*bam*), one of the few known
489 differentiation factors in *Drosophila* germ cells, is necessary for the transition from GSC to
490 cystoblast and for cystoblast divisions, at least in part because it stabilizes CycA expression in
491 dividing cysts (Ji et al., 2017). CycA/Cdk1 activity is further controlled at the level of translation
492 and ubiquitin-mediated proteolysis. Cyclin/Cdk protein levels and activity are very high in early
493 cyst divisions but decrease as cysts approach the terminal mitotic division (Hinnant et al., 2017;
494 Lilly et al., 2000). Since cystoblasts divide exactly four times, several prior studies posited the
495 model that cystoblasts autonomously limit the number of divisions through a molecular counting
496 mechanism that involves Bam, CycA, and the fusome (Hinnant et al., 2020; Huynh, 2006; Ji et al.,
497 2017; King, 1970; Lilly et al., 2000; McKearin, 1997). While a counting mechanism would limit
498 the number of mitotic divisions, it must also promote modification of contractile ring proteins to
499 block cytokinesis, stabilize intercellular bridges into stable ring canals, and maintain the
500 biosynthesis of the fusome (McKearin, 1997).

501 Our data suggest that the Ran/β-importin intracellular transport system is integrated into
502 the CycA-dependent cell division counting machinery. Depletion of *Ran*, *cdm*, or *Tnpo-SR*
503 generated egg chambers with abnormal numbers of cells (Table 1), some on the order of 2^n
504 reminiscent of cyclin mutants (Lilly et al., 2000; Mathieu et al., 2013; Morris et al., 2005;
505 Ohlmeyer and Schüpbach, 2003), and others deviating from this pattern, more similar to mutants
506 which disrupt intercellular bridge formation and fusome biogenesis (de Cuevas et al., 1996; Lin et
507 al., 1994; Yue and Spradling, 1992). Although we cannot establish a clear temporal sequence of
508 events mediated by Ran from our current data, we envision two possible mechanisms of action.
509 We favor the hypothesis that Ran mediates intracellular movement of CycA itself or a factor that
510 promotes CycA degradation. Binding by Tnpo-SR or Cdm could sequester the cell cycle regulator,
511 preventing activation by sterically inhibiting interaction with a kinase or by blocking protein
512 accumulation at the fusome. High levels of Ran-GTP levels would promote release of the Tnpo-

513 SR cargo, freeing it for activation. In the absence of Tnpo-SR or Cdm, where mitotic regulators
514 cannot be delivered to Ran, CycA levels instead accumulate at the fusome and in the cytoplasm,
515 promoting continued mitotic division. Alternatively, Ran-GTP could regulate contractile protein
516 localization and cell polarization, as has been demonstrated for human Ran in mammalian somatic
517 cells (Beaudet et al., 2017; Silverman-Gavrila et al., 2008). Although we do not detect clear
518 evidence of altered cytokinesis or failure to properly localize Anillin to ring canals in the dominant
519 negative *Ran*^{T24N} mutant, it is possible that our immunofluorescence assay is not sensitive enough
520 to detect such defects. Indeed, we have been unable to visualize the cortical accumulation of
521 Anillin in dividing germ cells described by previous studies (de Cuevas and Spradling, 1998) using
522 the anti-Anillin or *UASp-Anillin-GFP* reagents available to us.
523
524 ***Tnpo-SR and Cdm may have Ran-independent roles in promoting cyst development.***
525 During nucleocytoplasmic transport, an α-importin/β-importin complex or individual β-
526 importin binds to a cargo in the cytoplasm and transports it across a nuclear pore (Barbato et al.,
527 2020; Görlich et al., 1997). Inside the nucleus, Ran-GTP binds to the complex, dissociating the
528 cargo from the importin. Given the close association between Ran and β-importins, we
529 hypothesized that depletion of *Ran* by RNAi, or over-expression of dominant negative Ran^{T24N}
530 mutant would phenocopy β-importin depletion. While this held true for GSC maintenance, cyst
531 division, and oocyte specification, we were surprised to find that fusome biogenesis defects, cyst
532 fragmentation, and delayed ring canal maturation phenotypes were unique to loss of *Tnpo-SR* and
533 *cdm*. Moreover, the constitutively active Ran^{Q69L} mutant, in which Ran is locked in a GTP-bound
534 configuration and should deplete the amount of free β-importin in cells, did not have severe defects
535 in germ cell mitoses. These results could indicate Ran-independent functions of Tnpo-SR and Cdm
536 in mitotically dividing germ cells. Based on molecular markers of the fusome and ring canals, we
537 conclude that in *Tnpo-SR*- and *Cdm*- depleted germ cells, the transition from mitosis to meiosis is
538 abrogated or delayed, such that cell-to-cell connections are not maintained. Delayed maturation of
539 the fusomes and ring canals appears to create weak connections between cells, resulting in
540 premature abscission or collapsed intercellular bridges (Figure 6M). Interestingly, we see fusomes
541 that are fragile and unbranched in structure (Figure 5E-H), but also germline tumors containing
542 cells with immature fusome morphology resembling that of 2-cell cysts (Figure 2G-H). This may
543 be the result of altered timing or different concentrations of the β-importins in the first division of

544 the cystoblast versus the remaining three, perhaps reflecting differing sensitivity to abscission
545 across the mitotic divisions (Mathieu et al., 2013; McKearin and Ohlstein, 1995). Cyst cell
546 fusomes are composed of endoplasmic reticulum-like vesicles and cytoskeletal elements that
547 originate from remnants of the mitotic spindle midbody (de Cuevas and Spradling, 1998; Koch
548 and King, 1966; Koch et al., 1967; Lin and Spradling, 1995; Mahowald, 1971). We speculate that
549 Tnpo-SR and Cdm promote reorganization of the germ cell cytoskeleton after mitotic division,
550 perhaps by shuttling cytoskeletal proteins back to the fusome. Although fusome biogenesis has not
551 been well-studied, it is clearly integral to cyst formation. Our study provides novel reagents to
552 further interrogate the molecular mechanisms promoting cyst interconnectivity.
553
554 ***Ran-GTP and β-importins may function as a conserved molecular timer for the mitotic-to-***
555 ***meiotic transition.***
556 The basic steps in cyst formation have been well described at the morphological level,
557 particularly in insects (de Cuevas et al., 1997; Lu et al., 2017; Pepling and Lei, 2018; Yamashita,
558 2018). Yet how cyst formation is guided molecularly remains an open area for study. Insects
559 provide excellent models, as many exhibit unique mechanisms for achieving cyst formation
560 (Büning, 1994; de Cuevas et al., 1997; Eastin et al., 2020; Kubrakiewicz, 1997). Given the level
561 of conservation in cell cycle control across species, we propose that Ran and β-importins may also
562 play important roles in higher eukaryotes, connecting the intricate programs of cell division, oocyte
563 differentiation, and cell polarization. This may be of particular consequence for mouse and human
564 oocytes, in which cyst breakdown occurs prior to meiotic onset (Pepling and Lei, 2018).
565 Understanding how Ran and importins control cyst formation and breakdown may help elucidate
566 how the oocyte reserve is established in humans, offering new potential avenues for treatment of
567 infertility.
568
569 **MATERIALS AND METHODS**
570 ***Drosophila strains and husbandry***
571 Flies were maintained at 22°-25°C in standard medium (cornmeal/molasses/yeast/agar)
572 (NutriFly MF; Genesee Scientific). Female progeny were collected one to two days after eclosion
573 and maintained on standard medium for 3, 6, and 10 days at 25°C; flies were fed wet yeast paste

574 for 2-3 days (changed daily) prior to ovary dissection. A complete list of fly lines used in this study
575 are provided in Supp. Table S1.
576
577 ***Tissue-specific RNA interference (RNAi) generation***
578 All RNAi lines used in this study were carried in *pVALIUM20* or *pVALIUM22* transposons
579 for maximum germline efficiency (Supp. Table S1). *UAS-Tnpo-SR*^{V22} was generated as described
580 (www.flyrnai.org/TRiP-HOME.html) (Ni et al., 2011). Primers were designed against the full-
581 length *Tnpo-SR* RNA via the Designer of Small Interfering RNA tool
582 (http://biodev.extra.cea.fr/DSIR/DSIRhtml) using default settings (21 nt siRNA; score threshold
583 90). A sequence with a score of 94.6 and 0 predicted off-targets was selected for hairpin generation
584 (passenger strand, CGATCCCGTTTACTGGATAGA; guide strand,
585 TCTATCCAGTAAACGGGATC). Primers were designed according to TRiP recommendations,
586 annealed to form double-stranded oligos, and ligated into EcoRI-HF/NheI-HF-digested
587 *pVALIUM22*. Transgenic flies (*UAS-Tnpo-SR*^{V22}) were generated by phiC31 site-specific integrase
588 into the *attP2* site on the third chromosome.
589 For RNAi experiments, germline knock-down was facilitated by expressing the germline-
590 specific *nos-GAL4::VP16-nos.UTR* (referred to throughout as *nos-Gal4*) (Rørth, 1998; Van Doren
591 et al., 1998). Driver expression was confirmed using *w*; nos-Gal4, UASp-tubGFP* (BDSC #7253)
592 (Grieder et al., 2000). Females carrying *nos-Gal4* alone were used as controls.
593
594 ***Drosophila genetic mosaic generation***
595 For genetic mosaic analyses using *flippase (FLP)/FLP recognition target (FRT)*, we
596 obtained the following mutant alleles of *FRT*-containing chromosome arms: *Tnpo-SR*^{KG04870}
597 [Kyoto *Drosophila* Stock Center (KDSC) #111581] (Bellen et al., 2004) and *Tnpo-SR*^{LL05552}
598 (KDSC #141628) (Schuldiner et al., 2008). Other genetic tools are described in FlyBase version
599 FB2020_05 (Thurmond et al., 2019). Genetic mosaics were generated by *FLP*/*FRT*-mediated
600 recombination in 2-3-day old females carrying a mutant allele in trans to a wildtype allele (linked
601 to a *Ubi-GFP* marker) on homologous *FRT* arms, and a *hs-FLP* transgene, as described (Laws and
602 Drummond-Barbosa, 2015). Flies were heat shocked at 37°C two times per day for 3 days and
603 incubated at 25°C for 4, 8, or 12 days and supplemented with wet yeast paste on the last 2 days
604 prior to dissection. Wild-type alleles were used for the generation of control (mock) mosaics.

605

606 ***Germ cell analyses***

607 GSCs were identified based on the juxtaposition of their fusomes to the junction with
608 adjacent cap cells (de Cuevas and Spradling, 1998). In *FLP*/*FRT* mutants, GSC loss was measured
609 two ways. First, as the percentage of total mosaic germaria showing evidence of recent stem cell
610 loss; namely, the presence of GFP-negative daughters (cystoblasts/cysts generated from an original
611 GFP-negative stem cell) in the absence of the GFP-negative mother stem cell (Laws and
612 Drummond-Barbosa, 2015). Second, as the percentage of total germaria analyzed that had at least
613 one GFP-negative GSC. All results were subjected to Chi-Square analyses using Microsoft Excel.
614 In RNAi progeny, GSC loss was measured as the average number of GSCs present over three
615 timepoints. Results were subjected to Student's two-tailed T-test comparing driver controls versus
616 *driver>UAS-RNAi* experimental groups at each timepoint individually using Microsoft Excel.

617 For analyses involving the egg chambers outside of the germarium, data was collected from
618 the first three egg chambers posteriorly located from the germarium. Oocytes were identified by
619 the presence of anti-Orb antibodies. The number of cells and ring canals per egg chamber were
620 calculated based on visualization of ring canals with anti-pTyr and/or anti-Hts-RC antibodies and
621 cell nuclei with DAPI. Results were subjected to Student's two-tailed T-test comparing driver
622 controls versus *driver>UAS-RNAi* experimental groups at each timepoint individually using
623 Microsoft Excel and Prism (GraphPad).

624

625 ***Immunofluorescence and microscopy***

626 Ovaries were prepared for immunofluorescence microscopy as described (Grieder et al.,
627 2000; Hinnant et al., 2017). In the standard protocol, ovaries were dissected and teased apart in
628 Grace's medium without additives (Caisson Labs) and fixed in 5.3% formaldehyde in Grace's
629 medium for 13 minutes at room temperature. They were then washed extensively in phosphate-
630 buffered saline (PBS, pH 7.4; Fisher) with 0.1% Triton X-100, and blocked for three hours in
631 blocking solution [5% bovine serum albumin (Sigma), 5% normal goat serum (MP Biomedicals),
632 and 0.1% Triton X-100 in PBS] at room temperature. To detect cells in S phase, dissected ovaries
633 were incubated for one hour at room temperature in Grace's media containing 10 μM 5-ethynyl-
634 2′-deoxyuridine (EdU; Life Technologies). The following primary antibodies were diluted in
635 blocking solution and used overnight at 4°C: chicken anti-GFP (#13970, Abcam; 1:2000), rabbit

636 anti-dsRed (#632496, Clontech; 1:500), rabbit anti-phosphoHistone H3 (pHH3; #06-570,
637 Millipore; 1:200), rat anti-E-Cadherin (DCAD2, Developmental Studies Hybridoma Bank
638 (DSHB); 1:20), mouse anti-Orb (4H8 and 6H4; DSHB; 1:500), mouse anti-BicD (1B11 and 4C2;
639 DSHB; 1:10), mouse anti-p-Tyrosine (Millipore; 1:100), mouse anti-Hts-RC (DSHB; 1:10),
640 mouse anti-CycA (A12; DSHB; 1:50), rabbit anti-C(3)G (a gift from M. Lilly; 1:3000), rat anti-
641 HA (3F10; Sigma; 1:25), mouse anti-α-Tubulin-AF555 (DM1A-AF555; Millipore; 1:100), and
642 rabbit anti-Anillin (a gift from J. Brill; 1:50). Mouse anti-Sxl (m18; DSHB; 1:500) was also used
643 but fixed in a 4% formaldehyde in Grace's medium. Primary antibodies mouse anti-Hts (1B1,
644 DSHB; 1:10), and mouse anti-Lamin C (LC28.26, DSHB; 1:100) were incubated over two nights
645 at 4°C. All primary antibodies are followed by a two hour incubation at room temperature with
646 AlexaFluor 488-, 568- or 633-conjugated goat species-specific secondary antibodies (Life
647 Technologies; 1:200). EdU was detected (if necessary) using AlexaFluor-594 or -647 via Click-
648 It chemistry, following the manufacturer's recommendations (Life Technologies).
649 For stabilizing structures such as mitotic spindles, ovaries were dissected and teased apart
650 in room temperature equilibrated Grace's medium and fixed for 10 minutes at room temperature
651 using 350µl Grace's Medium and 200µl of 16% formaldehyde. They were then extensively washed
652 in PBS with 0.1% Triton X-100 and blocked at room temperature for at least 30 minutes in
653 blocking solution (2.5mL NGS, 5mL Triton, 42.5mL 1xPBS). Primary antibody incubations took
654 place overnight at 4°C followed by extensive washing in PBS with 0.1% Triton X-100 and another
655 blocking period of at least 30 minutes at room temperature. Detection of secondary antibodies
656 proceeded as described above.
657 All ovary samples were stained with 0.5 µg/ml 4'-6-diamidino-2-phenylindole (DAPI;
658 Sigma) in 0.1% Triton X-100 in PBS, and mounted in 90% glycerol mixed with 20% n-propyl
659 gallate (Sigma). Confocal z-stacks (1 µm optical sections) were collected with either the Zeiss
660 LSM700 laser scanning microscope using ZEN Black 2012 software or the Zeiss LSM800 laser
661 scanning microscope using ZEN Blue 2012. Images were analyzed using Zeiss ZEN software, and
662 minimally and equally enhanced via histogram using ZEN and Adobe Photoshop Creative Suite.
663

664 **ACKNOWLEDGMENTS**

665 Many thanks to K. McKim (Rutgers University), B. Riggs (San Francisco State University), K.
666 Roper (University of Cambridge), J.-Q. Ni (Tsinghua University), M. Lilly (NICHD), D.

Drummond-Barbosa (Johns Hopkins University), M. Buszczak (University of Texas Southwestern Medical Center), L. Cooley (Yale University), and J. Brill (University of Toronto) for their kind gifts of fly stocks and antibodies. We would also like to thank the East Carolina University School of Dental Medicine for use of their Zeiss LSM800 microscope. We are grateful to the Bloomington *Drosophila* Stock Center and Genomics Resource Center, the Vienna *Drosophila* Resource Center, the Kyoto *Drosophila* Genomics and Genetic Resources Center, the Transgenic RNAi Project at Harvard Medical School, the University of Iowa Developmental Studies Hybridoma Bank for making other fly lines, antibodies, and plasmids available, and BestGene for *Drosophila* transgenesis and screening. Many thanks to Tianna Van Cura and members of the Ables laboratory for assistance with building tools, providing helpful discussions, and critical reading of this manuscript.

COMPETING INTERESTS

The authors declare no competing conflicts of interest.

FUNDING

This work was supported by National Institutes of Health R15-GM117502 (E. T. A.), the East Carolina University (ECU) Division of Research and Graduate Studies (A. N. B. and T. D. H.), the ECU Office of Undergraduate Research (A. E. W.), and the ECU Honors College (A. M. P.).

DATA AVAILABILITY

Fly strains and plasmids are available upon request. The authors affirm that all data necessary for confirming the conclusions of the article are present within the article and figures.

REFERENCES

Ables, E. T. and Drummond-Barbosa, D. (2013). Cyclin E controls Drosophila female germline stem cell maintenance independently of its role in proliferation by modulating responsiveness to niche signals. *Development* **140**, 530-540.

Ables, E. T., Hwang, G. H., Finger, D. S., Hinnant, T. D. and Drummond-Barbosa, D. (2016). A Genetic Mosaic Screen Reveals Ecdysone-Responsive Genes Regulating Drosophila Oogenesis. *G3 (Bethesda, Md.)* **6**, 2629-2642.

Allemand, E., Dokudovskaya, S., Bordonné, R. and Tazi, J. (2002). A conserved Drosophila transportin-serine/arginine-rich (SR) protein permits nuclear import of Drosophila SR protein splicing factors and their antagonist repressor splicing factor 1. *Molecular biology of the cell* **13**, 2436-2447.

701 **Ameku, T. and Niwa, R.** (2016). Mating-Induced Increase in Germline Stem Cells via the Neuroendocrine
702 System in Female Drosophila. *PLoS genetics* **12**, e1006123.
703 **Barbato, S., Kapinos, L. E., Rencurel, C. and Lim, R. Y. H.** (2020). Karyopherin enrichment at the nuclear
704 pore complex attenuates Ran permeability. *J Cell Sci* **133**.
705 **Beaudet, D., Akhshi, T., Phillipp, J., Law, C. and Piekny, A.** (2017). Active Ran regulates anillin function
706 during cytokinesis. *Molecular biology of the cell* **28**, 3517-3531.
707 **Beaudet, D., Pham, N., Skaik, N. and Piekny, A.** (2020). Importin binding mediates the intramolecular
708 regulation of anillin during cytokinesis. *Molecular biology of the cell* **31**, 1124-1139.
709 **Bellen, H. J., Levis, R. W., Liao, G., He, Y., Carlson, J. W., Tsang, G., Evans-Holm, M., Hiesinger, P. R.,**
710 **Schulze, K. L., Rubin, G. M., et al.** (2004). The BDGP gene disruption project: single transposon
711 insertions associated with 40% of Drosophila genes. *Genetics* **167**, 761-781.
712 **Bradley, T., Cook, M. E. and Blanchette, M.** (2015). SR proteins control a complex network of RNA-
713 processing events. *Rna* **21**, 75-92.
714 **Büning, J.** (1994). *The Insect Ovary: Ultrastructure, previtellogenic growth and evolution*: Springer,
715 Dordrecht.
716 **Buszczak, M., Paterno, S., Lighthouse, D., Bachman, J., Planck, J., Owen, S., Skora, A. D., Nystul, T. G.,**
717 **Ohlstein, B., Allen, A., et al.** (2007). The carnegie protein trap library: a versatile tool for
718 Drosophila developmental studies. *Genetics* **175**, 1505-1531.
719 **Cautain, B., Hill, R., de Pedro, N. and Link, W.** (2015). Components and regulation of nuclear transport
720 processes. *The FEBS journal* **282**, 445-462.
721 **Cesario, J. and McKim, K. S.** (2011). RanGTP is required for meiotic spindle organization and the
722 initiation of embryonic development in Drosophila. *J Cell Sci* **124**, 3797-3810.
723 **Chaigne, A., Labouesse, C., White, I. J., Agnew, M., Hannezo, E., Chalut, K. J. and Paluch, E. K.** (2020).
724 Abscission Couples Cell Division to Embryonic Stem Cell Fate. *Developmental cell* **55**, 195-
725 208.e195.
726 **Chang, C. C. and Hsia, K. C.** (2020). More than a zip code: global modulation of cellular function by
727 nuclear localization signals. *The FEBS journal*.
728 **Chau, J., Kulnane, L. S. and Salz, H. K.** (2009). Sex-lethal facilitates the transition from germline stem cell
729 to committed daughter cell in the Drosophila ovary. *Genetics* **182**, 121-132.
730 **Chen, A., Akhshi, T. K., Lavoie, B. D. and Wilde, A.** (2015). Importin β2 Mediates the Spatio-temporal
731 Regulation of Anillin through a Noncanonical Nuclear Localization Signal. *The Journal of*
732 *biological chemistry* **290**, 13500-13509.
733 **Chen, D., Wang, Q., Huang, H., Xia, L., Jiang, X., Kan, L., Sun, Q. and Chen, D.** (2009). Effete-mediated
734 degradation of Cyclin A is essential for the maintenance of germline stem cells in Drosophila.
735 *Development* **136**, 4133-4142.
736 **Chen, J., Call, G. B., Beyer, E., Bui, C., Cespedes, A., Chan, A., Chan, J., Chan, S., Chhabra, A., Dang, P.,**
737 **et al.** (2005). Discovery-based science education: functional genomic dissection in Drosophila by
738 undergraduate researchers. *PLoS Biol* **3**, e59.
739 **Cheng, J., Türkel, N., Hemati, N., Fuller, M. T., Hunt, A. J. and Yamashita, Y. M.** (2008). Centrosome
740 misorientation reduces stem cell division during ageing. *Nature* **456**, 599-604.
741 **de Cuevas, M., Lee, J. K. and Spradling, A. C.** (1996). alpha-spectrin is required for germline cell division
742 and differentiation in the Drosophila ovary. *Development* **122**, 3959-3968.
743 **de Cuevas, M., Lilly, M. A. and Spradling, A. C.** (1997). Germline cyst formation in Drosophila. *Annual*
744 *review of genetics* **31**, 405-428.
745 **de Cuevas, M. and Spradling, A. C.** (1998). Morphogenesis of the Drosophila fusome and its implications
746 for oocyte specification. *Development* **125**, 2781-2789.

Deng, W. and Lin, H. (1997). Spectrosomes and fusomes anchor mitotic spindles during asymmetric germ cell divisions and facilitate the formation of a polarized microtubule array for oocyte specification in Drosophila. *Developmental biology* **189**, 79-94.

Drutovic, D., Duan, X., Li, R., Kalab, P. and Solc, P. (2020). RanGTP and importin β regulate meiosis I spindle assembly and function in mouse oocytes. *The EMBO journal* **39**, e101689.

Eastin, K. J., Huang, A. P. and Ferree, P. M. (2020). A novel pattern of germ cell divisions in the production of hymenopteran insect eggs. *Biol Lett* **16**, 20200137.

Eikenes Å, H., Malerød, L., Lie-Jensen, A., Sem Wegner, C., Brech, A., Liestøl, K., Stenmark, H. and Haglund, K. (2015). Src64 controls a novel actin network required for proper ring canal formation in the Drosophila male germline. *Development* **142**, 4107-4118.

Fichelson, P., Jagut, M., Lepanse, S., Lepesant, J. A. and Huynh, J. R. (2010). lethal giant larvae is required with the par genes for the early polarization of the Drosophila oocyte. *Development* **137**, 815-824.

Forbes, D. J., Travesa, A., Nord, M. S. and Bernis, C. (2015). Nuclear transport factors: global regulation of mitosis. *Current opinion in cell biology* **35**, 78-90.

Frémont, S. and Echard, A. (2018). Membrane Traffic in the Late Steps of Cytokinesis. *Current biology : CB* **28**, R458-R470.

Geles, K. G. and Adam, S. A. (2001). Germline and developmental roles of the nuclear transport factor importin alpha3 in C. elegans. *Development* **128**, 1817-1830.

Goldbach, P., Wong, R., Beise, N., Sarpal, R., Trimble, W. S. and Brill, J. A. (2010). Stabilization of the actomyosin ring enables spermatocyte cytokinesis in Drosophila. *Molecular biology of the cell* **21**, 1482-1493.

Görlich, D., Dabrowski, M., Bischoff, F. R., Kutay, U., Bork, P., Hartmann, E., Prehn, S. and Izaurralde, E. (1997). A novel class of RanGTP binding proteins. *J Cell Biol* **138**, 65-80.

Grieder, N. C., de Cuevas, M. and Spradling, A. C. (2000). The fusome organizes the microtubule network during oocyte differentiation in Drosophila. *Development* **127**, 4253-4264.

Guertin, D. A., Trautmann, S. and McCollum, D. (2002). Cytokinesis in eukaryotes. *Microbiology and molecular biology reviews : MMBR* **66**, 155-178.

Haglund, K., Nezis, I. P. and Stenmark, H. (2011). Structure and functions of stable intercellular bridges formed by incomplete cytokinesis during development. *Communicative & integrative biology* **4**, 1-9.

Hinnant, T. D., Alvarez, A. A. and Ables, E. T. (2017). Temporal remodeling of the cell cycle accompanies differentiation in the Drosophila germline. *Developmental biology* **429**, 118-131.

Hinnant, T. D., Merkle, J. A. and Ables, E. T. (2020). Coordinating Proliferation, Polarity, and Cell Fate in the Drosophila Female Germline. *Frontiers in cell and developmental biology* **8**, 19.

Hogarth, C., Itman, C., Jans, D. A. and Loveland, K. L. (2005). Regulated nucleocytoplasmic transport in spermatogenesis: a driver of cellular differentiation? *BioEssays : news and reviews in molecular, cellular and developmental biology* **27**, 1011-1025.

Hughes, S. E., Miller, D. E., Miller, A. L. and Hawley, R. S. (2018). Female Meiosis: Synapsis, Recombination, and Segregation in Drosophila melanogaster. *Genetics* **208**, 875-908.

Huynh, J.-R. (2006). Fusome as a Cell-Cell Communication Channel of Drosophila Ovarian Cyst. In *Cell-Cell Channels* (ed. F. Baluska, D. Volkmann & P. W. Barlow), pp. 217-235. New York, NY: Springer New York.

Ji, S., Li, C., Hu, L., Liu, K., Mei, J., Luo, Y., Tao, Y., Xia, Z., Sun, Q. and Chen, D. (2017). Bam-dependent deubiquitinase complex can disrupt germ-line stem cell maintenance by targeting cyclin A. *Proceedings of the National Academy of Sciences of the United States of America* **114**, 6316-6321.

Kimura, M. and Imamoto, N. (2014). Biological significance of the importin-β family-dependent nucleocytoplasmic transport pathways. *Traffic (Copenhagen, Denmark)* **15**, 727-748.

Kimura, M., Morinaka, Y., Imai, K., Kose, S., Horton, P. and Imamoto, N. (2017). Extensive cargo identification reveals distinct biological roles of the 12 importin pathways. *eLife* **6**.

King, R. C. R. C. (1970). Ovarian development in Drosophila melanogaster. New York: Academic Press.

Koch, E. A. and King, R. C. (1966). The origin and early differentiation of the egg chamber of Drosophila melanogaster. *J Morphol* **119**, 283-303.

Koch, E. A., Smith, P. A. and King, R. C. (1967). The division and differentiation of Drosophila cystocytes. *J Morphol* **121**, 55-70.

Kosyna, F. K. and Depping, R. (2018). Controlling the Gatekeeper: Therapeutic Targeting of Nuclear Transport. *Cells* **7**.

Kubrakiewicz, J. (1997). Germ cells cluster organization in polytrophic ovaries of neuroptera. *Tissue and Cell* **29**, 221-228.

Lai, M. C., Lin, R. I. and Tarn, W. Y. (2001). Transportin-SR2 mediates nuclear import of phosphorylated SR proteins. *Proc Natl Acad Sci U S A* **98**, 10154-10159.

Laws, K. M. and Drummond-Barbosa, D. (2015). Genetic Mosaic Analysis of Stem Cell Lineages in the Drosophila Ovary. *Methods in molecular biology (Clifton, N.J.)* **1328**, 57-72.

Lighthouse, D. V., Buszczak, M. and Spradling, A. C. (2008). New components of the Drosophila fusome suggest it plays novel roles in signaling and transport. *Developmental biology* **317**, 59-71.

Lilly, M. A., de Cuevas, M. and Spradling, A. C. (2000). Cyclin A associates with the fusome during germline cyst formation in the Drosophila ovary. *Developmental biology* **218**, 53-63.

Lin, H. and Spradling, A. C. (1995). Fusome asymmetry and oocyte determination in Drosophila. *Dev Genet* **16**, 6-12.

Lin, H., Yue, L. and Spradling, A. C. (1994). The Drosophila fusome, a germline-specific organelle, contains membrane skeletal proteins and functions in cyst formation. *Development* **120**, 947-956.

Lippai, M., Tirián, L., Boros, I., Mihály, J., Erdélyi, M., Belecz, I., Máthé, E., Pósfai, J., Nagy, A., Udvardy, A., et al. (2000). The Ketel gene encodes a Drosophila homologue of importin-beta. *Genetics* **156**, 1889-1900.

Liu, L., Michowski, W., Kolodziejczyk, A. and Sicinski, P. (2019). The cell cycle in stem cell proliferation, pluripotency and differentiation. *Nature cell biology* **21**, 1060-1067.

Loveland, K. L., Major, A. T., Butler, R., Young, J. C., Jans, D. A. and Miyamoto, Y. (2015). Putting things in place for fertilization: discovering roles for importin proteins in cell fate and spermatogenesis. *Asian journal of andrology* **17**, 537-544.

Lu, K., Jensen, L., Lei, L. and Yamashita, Y. M. (2017). Stay Connected: A Germ Cell Strategy. *Trends in genetics : TIG* **33**, 971-978.

Maertens, G. N., Cook, N. J., Wang, W., Hare, S., Gupta, S. S., Öztop, I., Lee, K., Pye, V. E., Cosnefroy, O., Snijders, A. P., et al. (2014). Structural basis for nuclear import of splicing factors by human Transportin 3. *Proc Natl Acad Sci U S A* **111**, 2728-2733.

Mahowald, A. P. (1971). The formation of ring canals by cell furrows in Drosophila. *Z Zellforsch Mikrosk Anat* **118**, 162-167.

Mason, D. A., Fleming, R. J. and Goldfarb, D. S. (2002). Drosophila melanogaster importin alpha1 and alpha3 can replace importin alpha2 during spermatogenesis but not oogenesis. *Genetics* **161**, 157-170.

Máthé, E., Bates, H., Huikeshoven, H., Deák, P., Glover, D. M. and Cotterill, S. (2000). Importin-alpha3 is required at multiple stages of Drosophila development and has a role in the completion of oogenesis. *Developmental biology* **223**, 307-322.

841 **Máthé, E., Inoue, Y. H., Palframan, W., Brown, G. and Glover, D. M.** (2003). Orbit/Mast, the CLASP
842 orthologue of Drosophila, is required for asymmetric stem cell and cystocyte divisions and
843 development of the polarised microtubule network that interconnects oocyte and nurse cells
844 during oogenesis. *Development* **130**, 901-915.
845 **Mathieu, J., Cauvin, C., Moch, C., Radford, S. J., Sampaio, P., Perdigoto, C. N., Schweisguth, F., Bardin,**
846 **A. J., Sunkel, C. E., McKim, K., et al.** (2013). Aurora B and cyclin B have opposite effects on the
847 timing of cytokinesis abscission in Drosophila germ cells and in vertebrate somatic cells.
848 *Developmental cell* **26**, 250-265.
849 **Mathieu, J. and Huynh, J. R.** (2017). Monitoring complete and incomplete abscission in the germ line
850 stem cell lineage of Drosophila ovaries. *Methods in cell biology* **137**, 105-118.
851 **Matias, N. R., Mathieu, J. and Huynh, J. R.** (2015). Abscission is regulated by the ESCRT-III protein shrub
852 in Drosophila germline stem cells. *PLoS genetics* **11**, e1004653.
853 **Matova, N. and Cooley, L.** (2001). Comparative aspects of animal oogenesis. *Developmental biology*
854 **231**, 291-320.
855 **McKearin, D.** (1997). The Drosophila fusome, organelle biogenesis and germ cell differentiation: if you
856 build it. *BioEssays : news and reviews in molecular, cellular and developmental biology* **19**, 147-
857 152.
858 **McKearin, D. and Ohlstein, B.** (1995). A role for the Drosophila bag-of-marbles protein in the
859 differentiation of cystoblasts from germline stem cells. *Development* **121**, 2937-2947.
860 **Megraw, T. L. and Kaufman, T. C.** (2000). The centrosome in Drosophila oocyte development. *Current*
861 *topics in developmental biology* **49**, 385-407.
862 **Mihalas, B. P., Western, P. S., Loveland, K. L., McLaughlin, E. A. and Holt, J. E.** (2015). Changing
863 expression and subcellular distribution of karyopherins during murine oogenesis. *Reproduction*
864 *(Cambridge, England)* **150**, 485-496.
865 **Morris, J. Z., Hong, A., Lilly, M. A. and Lehmann, R.** (2005). twin, a CCR4 homolog, regulates cyclin
866 poly(A) tail length to permit Drosophila oogenesis. *Development* **132**, 1165-1174.
867 **Nguyen, L. T. S. and Robinson, D. N.** (2020). The Unusual Suspects in Cytokinesis: Fitting the Pieces
868 Together. *Frontiers in cell and developmental biology* **8**, 441.
869 **Ni, J. Q., Zhou, R., Czech, B., Liu, L. P., Holderbaum, L., Yang-Zhou, D., Shim, H. S., Tao, R., Handler, D.,**
870 **Karpowicz, P., et al.** (2011). A genome-scale shRNA resource for transgenic RNAi in Drosophila.
871 *Nat Methods* **8**, 405-407.
872 **Ohlmeyer, J. T. and Schüpbach, T.** (2003). Encore facilitates SCF-Ubiquitin-proteasome-dependent
873 proteolysis during Drosophila oogenesis. *Development* **130**, 6339-6349.
874 **Okada, N., Ishigami, Y., Suzuki, T., Kaneko, A., Yasui, K., Fukutomi, R. and Isemura, M.** (2008).
875 Importins and exportins in cellular differentiation. *J Cell Mol Med* **12**, 1863-1871.
876 **Ong, S. and Tan, C.** (2010). Germline cyst formation and incomplete cytokinesis during Drosophila
877 melanogaster oogenesis. *Developmental biology* **337**, 84-98.
878 **Ozugergin, I. and Piekny, A.** (2020). Complementary functions for the Ran gradient during division.
879 *Small GTPases*, 1-11.
880 **Pan, L., Chen, S., Weng, C., Call, G., Zhu, D., Tang, H., Zhang, N. and Xie, T.** (2007). Stem cell aging is
881 controlled both intrinsically and extrinsically in the Drosophila ovary. *Cell Stem Cell* **1**, 458-469.
882 **Pepling, M. and Lei, L.** (2018). Germ Cell Nests and Germline Cysts. In *Encyclopedia of Reproduction*
883 *(Second Edition)* (ed. M. K. Skinner), pp. 159-166. Oxford: Academic Press.
884 **Pepling, M. E., de Cuevas, M. and Spradling, A. C.** (1999). Germline cysts: a conserved phase of germ
885 cell development? *Trends in Cell Biology* **9**, 257-262.
886 **Perkins, L. A., Holderbaum, L., Tao, R., Hu, Y., Sopko, R., McCall, K., Yang-Zhou, D., Flockhart, I., Binari,**
887 **R., Shim, H. S., et al.** (2015). The Transgenic RNAi Project at Harvard Medical School: Resources
888 and Validation. *Genetics* **201**, 843-852.

Petrella, L. N., Smith-Leiker, T. and Cooley, L. (2007). The Ovhts polyprotein is cleaved to produce fusome and ring canal proteins required for Drosophila oogenesis. *Development* **134**, 703-712.

Piekny, A. J. and Maddox, A. S. (2010). The myriad roles of Anillin during cytokinesis. *Seminars in cell & developmental biology* **21**, 881-891.

Pollard, T. D. and O'Shaughnessy, B. (2019). Molecular Mechanism of Cytokinesis. *Annu Rev Biochem* **88**, 661-689.

Robinson, D. N., Cant, K. and Cooley, L. (1994). Morphogenesis of Drosophila ovarian ring canals. *Development* **120**, 2015-2025.

Röper, K. (2007). Rtnl1 is enriched in a specialized germline ER that associates with ribonucleoprotein granule components. *J Cell Sci* **120**, 1081-1092.

Rørth, P. (1998). Gal4 in the Drosophila female germline. *Mech Dev* **78**, 113-118.

Sazer, S. and Dasso, M. (2000). The ran decathlon: multiple roles of Ran. *J Cell Sci* **113 (Pt 7)**, 1111-1118.

Schuldiner, O., Berdnik, D., Levy, J. M., Wu, J. S., Luginbuhl, D., Gontang, A. C. and Luo, L. (2008). piggyBac-based mosaic screen identifies a postmitotic function for cohesin in regulating developmental axon pruning. *Developmental cell* **14**, 227-238.

Silverman-Gavrila, R. V., Hales, K. G. and Wilde, A. (2008). Anillin-mediated targeting of peanut to pseudocleavage furrows is regulated by the GTPase Ran. *Molecular biology of the cell* **19**, 3735-3744.

Snapp, E. L., Iida, T., Frescas, D., Lippincott-Schwartz, J. and Lilly, M. A. (2004). The fusome mediates intercellular endoplasmic reticulum connectivity in Drosophila ovarian cysts. *Molecular biology of the cell* **15**, 4512-4521.

Storto, P. D. and King, R. C. (1989). The role of polyfusomes in generating branched chains of cystocytes during Drosophila oogenesis. *Dev Genet* **10**, 70-86.

Sugimura, I. and Lilly, M. A. (2006). Bruno inhibits the expression of mitotic cyclins during the prophase I meiotic arrest of Drosophila oocytes. *Developmental cell* **10**, 127-135.

Teixeira, F. K. and Lehmann, R. (2019). Translational Control during Developmental Transitions. *Cold Spring Harb Perspect Biol* **11**.

Thurmond, J., Goodman, J. L., Strelets, V. B., Attrill, H., Gramates, L. S., Marygold, S. J., Matthews, B. B., Millburn, G., Antonazzo, G., Trovisco, V., et al. (2019). FlyBase 2.0: the next generation. *Nucleic Acids Res* **47**, D759-d765.

Tirián, L., Puro, J., Erdélyi, M., Boros, I., Papp, B., Lippai, M. and Szabad, J. (2000). The Ketel(D) dominant-negative mutations identify maternal function of the Drosophila importin-beta gene required for cleavage nuclei formation. *Genetics* **156**, 1901-1912.

Trieselmann, N. and Wilde, A. (2002). Ran localizes around the microtubule spindle in vivo during mitosis in Drosophila embryos. *Current biology : CB* **12**, 1124-1129.

Van Doren, M., Williamson, A. L. and Lehmann, R. (1998). Regulation of zygotic gene expression in Drosophila primordial germ cells. *Current biology : CB* **8**, 243-246.

Villányi, Z., Debec, A., Timinszky, G., Tirián, L. and Szabad, J. (2008). Long persistence of importin-beta explains extended survival of cells and zygotes that lack the encoding gene. *Mech Dev* **125**, 196-206.

Xu, T. and Rubin, G. M. (1993). Analysis of genetic mosaics in developing and adult Drosophila tissues. *Development* **117**, 1223-1237.

Yamashita, Y. M. (2018). Subcellular Specialization and Organelle Behavior in Germ Cells. *Genetics* **208**, 19-51.

Yue, L. and Spradling, A. C. (1992). hu-li tai shao, a gene required for ring canal formation during Drosophila oogenesis, encodes a homolog of adducin. *Genes & development* **6**, 2443-2454.

935 **Zielke, N., Korzelius, J., van Straaten, M., Bender, K., Schuhknecht, G. F. P., Dutta, D., Xiang, J. and**
936 **Edgar, B. A.** (2014). Fly-FUCCI: A versatile tool for studying cell proliferation in complex tissues.
937 *Cell Rep* **7**, 588-598.

938

939

940

941 **TABLES**

942 **Table 1.** Frequency of egg chambers that do not follow the power of two rule in β-importin- and
943 Ran-depleted ovaries.

944

Genotype	% of egg chambers that do not follow 2^n germ cells
Driver control	0
Fs(2)Ket^{GL01273}	1.3
Ran^{GL01341}	2.6
cdm^{HMS02846}	55.0
Tnpo-SR^{V22}	29.3
Ran$^{HA\ (ins\ 1)}$	0
Ran$^{HA\ (ins\ 2)}$	0
Ran $^{T24N\ (ins\ 1)}$	12.5
Ran $^{T24N\ (ins\ 2)}$	9.7
Ran $^{Q69L\ (ins\ 1)}$	0
Ran $^{Q69L\ (ins\ 2)}$	2.2

945

946 **FIGURES**

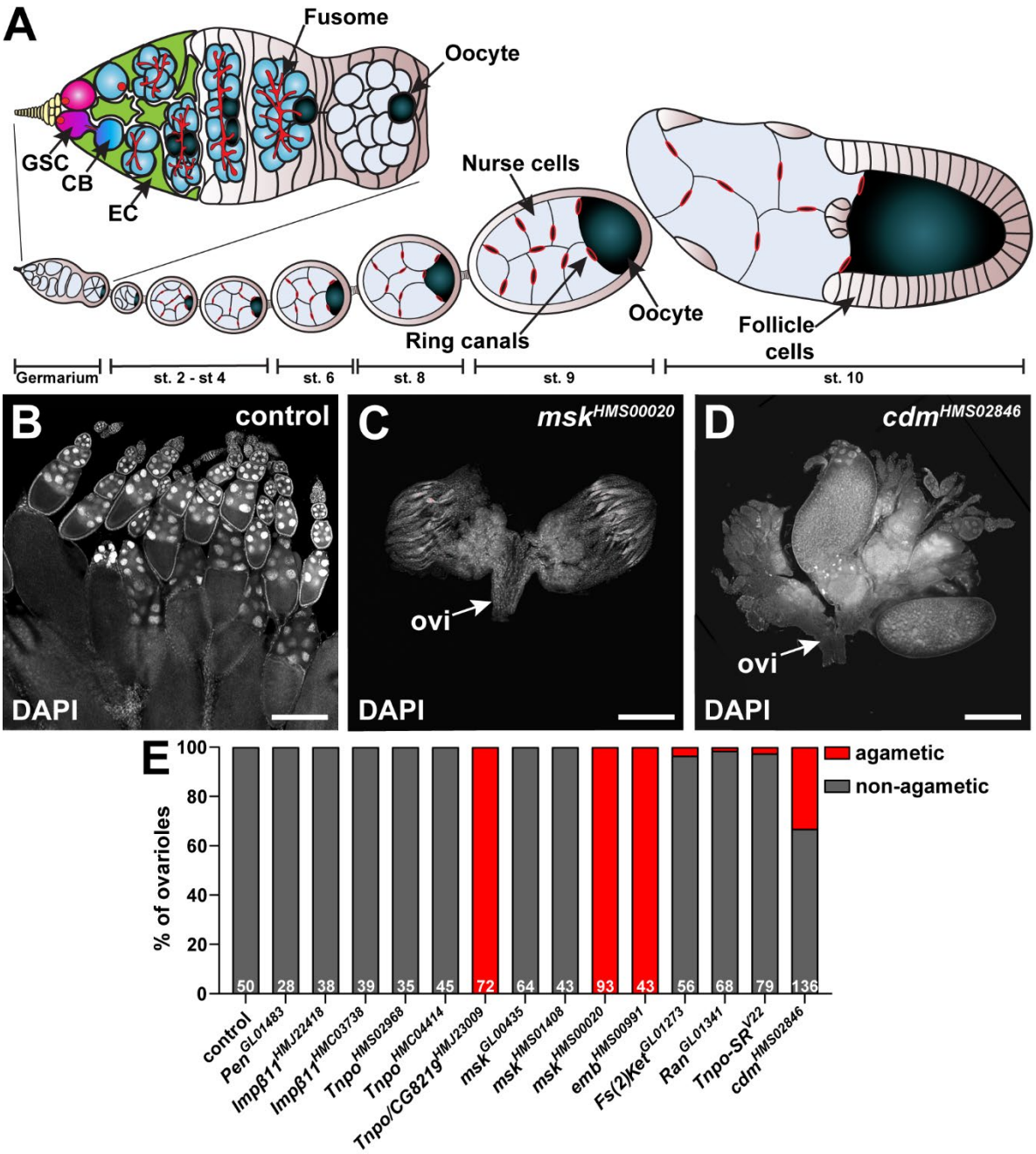

947

948 **Figure 1. An RNAi screen identified importins essential for germ cell development.**

949 (A) The *Drosophila* ovary is composed of 14-16 ovarioles, each harboring a germarium (top) and
950 older follicle cells that progress through 14 distinct stages of development (bottom). Within the
951 germarium, germline stem cells (GSCs; pink) are adjacent to cap cells (yellow) and a population
952 of escort cells (green). GSCs divide to form daughter cells (cystoblasts; blue) that go on to divide

953 four additional times to form 16-celled germline cysts (blue). Each cyst is composed of 15 nurse
954 cells and one oocyte (dark blue), connected by 15 intercellular bridges that can be visualized by
955 ring canals and the endoplasmic reticulum-like fusome (red) that transects each bridge. (B-D)
956 Maximum intensity projections of *nos-Gal4* control (B), *nos-Gal4>UAS- msk*^{HMS00020} (C), or *nos-*
957 *Gal4>UAS-cdm*^{HMS02846} (D) knockdown ovaries labeled with DAPI (white; nuclei). Scale bar, 100
958 µm. In control ovaries, each ovariole produces germline cysts that are packaged into individual
959 egg chambers. As egg chambers develop, oocytes grow and accumulate yolk, while nurse cells
960 become polyploid, adopting a stereotypical nuclear morphology. In *nos-Gal4>UAS-msk*^{HMS00020}
961 ovaries, ovarioles are present but completely lack germ cells. In *nos-Gal4>UAS-cdm*^{HMS02846}
962 ovaries, ovarioles have a partial agametic phenotype, where germ cells are present in some
963 ovarioles but ovaries are dramatically smaller than wild-type. Arrows indicate oviducts (ovi). (E)
964 Frequencies of ovarioles containing agametic (red) ovarioles. The number of ovarioles analyzed
965 is shown inside bars.
966

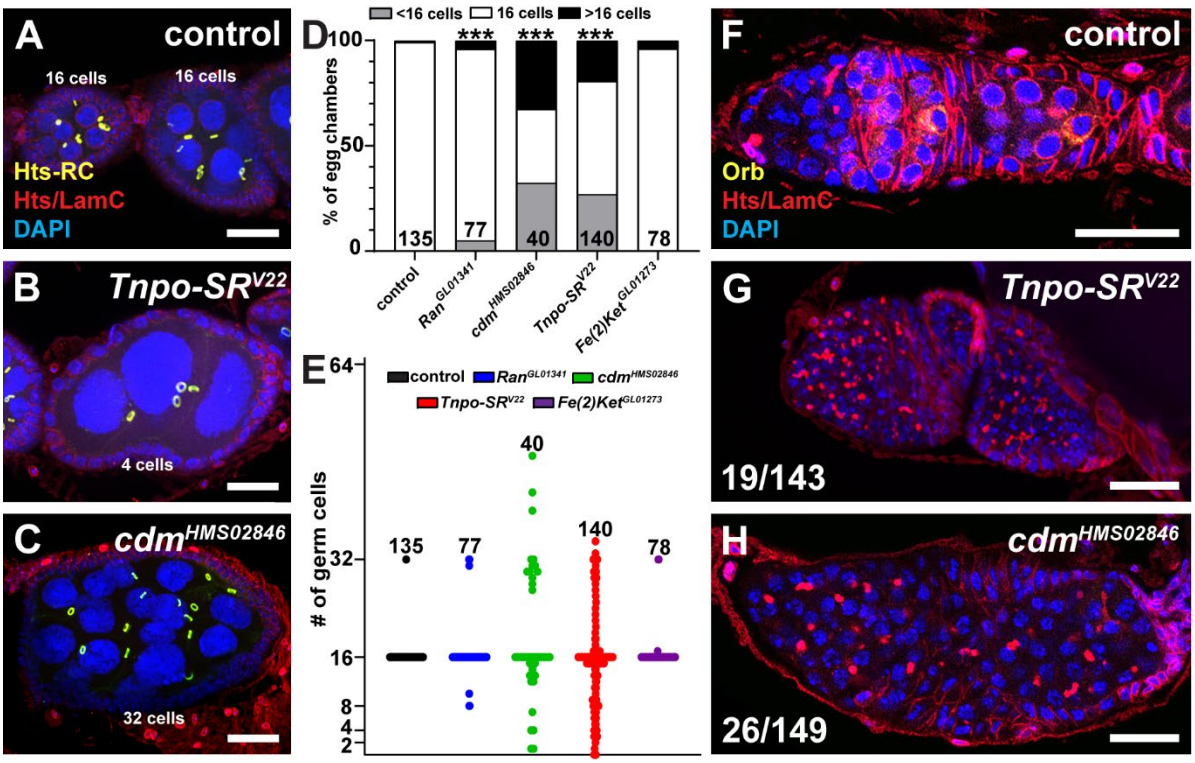

Figure 2. Ran and β-importins regulate the number of germ cells per egg chamber. (A-C) Egg chambers of driver control (A) or *nos-Gal4* driving RNAi against *Tnpo-SR* (B) and *cdm* (C) ovarioles labeled with anti-Hts-RC (yellow; ring canals), anti-Hts (red; fusomes and follicle cell membranes), anti-LamC (red; nuclear envelopes), and DAPI (blue; nuclei). (D) Frequencies of egg chambers containing less than 16 (grey), 16 (white), or more than 16 (black) germ cells per egg chamber in *nos-Gal4* control or *nos-Gal4* driving *Ran*, *cdm*, *Tnpo-SR*, or *Ketel* RNAi lines at 6 dae. (E) Variation of the number of germ cells per egg chambers. The numbers in/above the bars represent the total number of egg chambers analyzed. (F-H) Germaria from control (F), *nos-Gal4>Tnpo-SR*^{V22} (G), and *nos-Gal4>cdm*^{HMS02846} RNAi (H) females labeled with anti-Orb (yellow; oocyte), anti-Hts and anti-LamC (red), and DAPI (blue). Values in bottom left corner of G-H represent the number of ovarioles containing germline tumors over the total number of ovarioles analyzed. A-C and G are 10 µm subset maximum intensity projections. Scale bar, 20 µm. Error bars, mean ± SEM. ***$p < 0.001$; Chi-squares test.

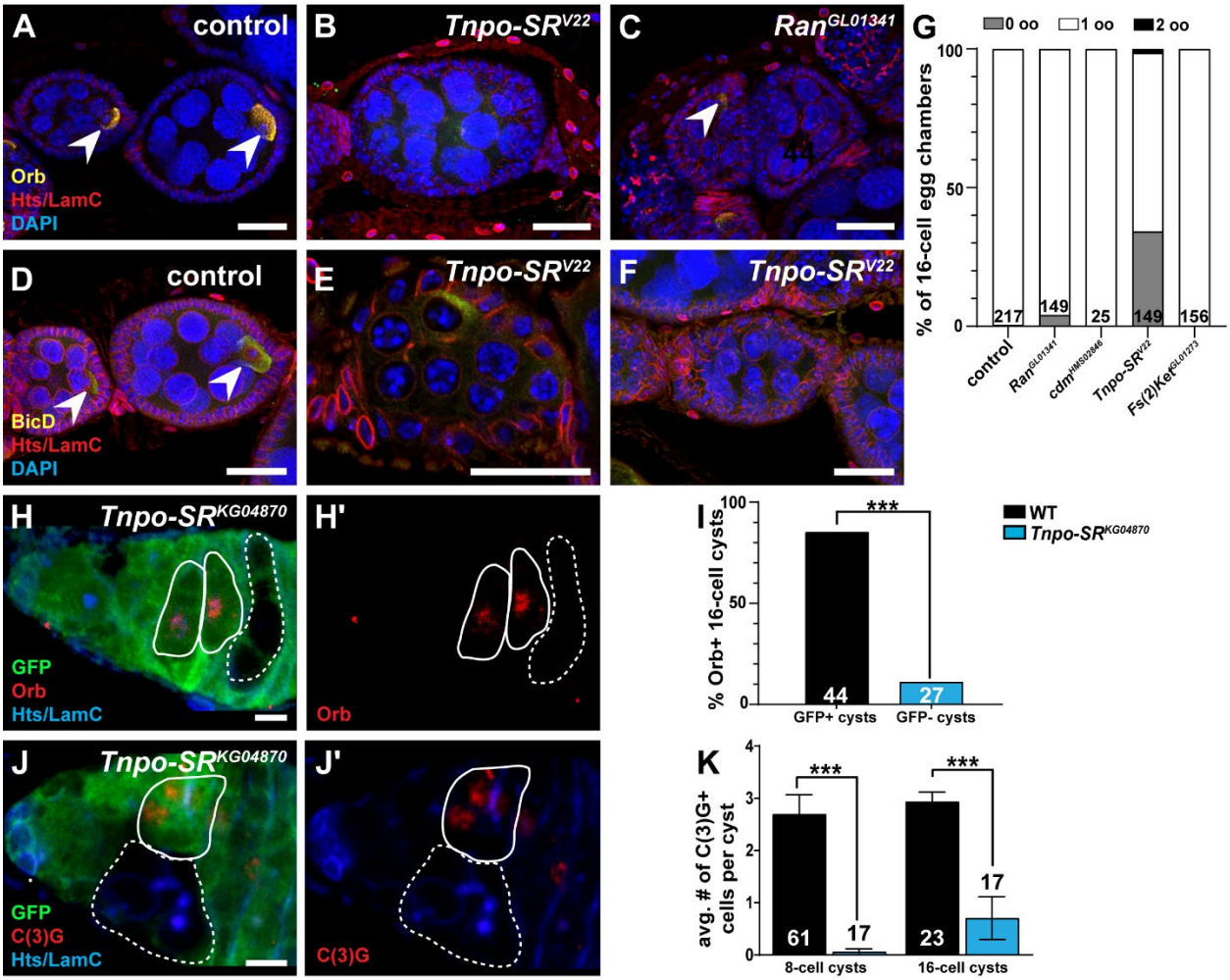

Figure 3. *Ran* and *Tnpo-SR* are required for proper oocyte selection.

(A-C) Driver control (A), *nosGal4>Tnpo-SR*^{V22} (B), and *nosGal4>Ran*^{GL01341} egg chambers labeled with anti-Orb (yellow; oocyte), anti-Hts (red; fusomes and follicle cell membranes), anti-LamC (red; nuclear envelopes), and DAPI (blue; nuclei). (D-F) Driver control (D) and *nosGal4>Tnpo-SR*^{V22} (E-F) egg chambers labeled with anti-BicD (yellow; oocyte), anti-Hts and anti-LamC (red), and DAPI (blue). Arrowheads indicate oocytes, recognized by their condensed nuclei. (G) Frequencies of egg chambers containing 0 (grey), 1 (white), or 2 (black) oocytes. The numbers in the bars represent the total number of egg chambers analyzed. (H-J) *Tnpo-SR*^{KG04870} mutant mosaic germarium at 8 days after clone induction labeled with anti-GFP (green; wild-type cells), anti-Hts and anti-LamC (blue), and anti-Orb (red) (H-H') or anti-C(3)G (red; synaptonemal complexes) (J-J'). White lines demarcate wild-type (solid) or mutant (dashed) cysts. (I) Percentage of GFP-positive (wild-type) or GFP-negative (*Tnpo-SR*^{KG04870}) 16-cell cysts with an Orb-positive

995 oocyte at 8 days after clone induction. (K) Average number of C(3)G-positive germ cells in GFP-
996 positive (wild-type) or GFP-negative (*Tnpo-SR*^{KG04870}) 8- or 16-cell cysts at 8 days after clone
997 induction. Numbers in the bars represent the total number of cysts analyzed. Scale bar, 20 µm (A-
998 F) and 5 µm (H-J). Error bars, mean ± SEM. ***$p < 0.001$; Student's two-tailed T-test.
999

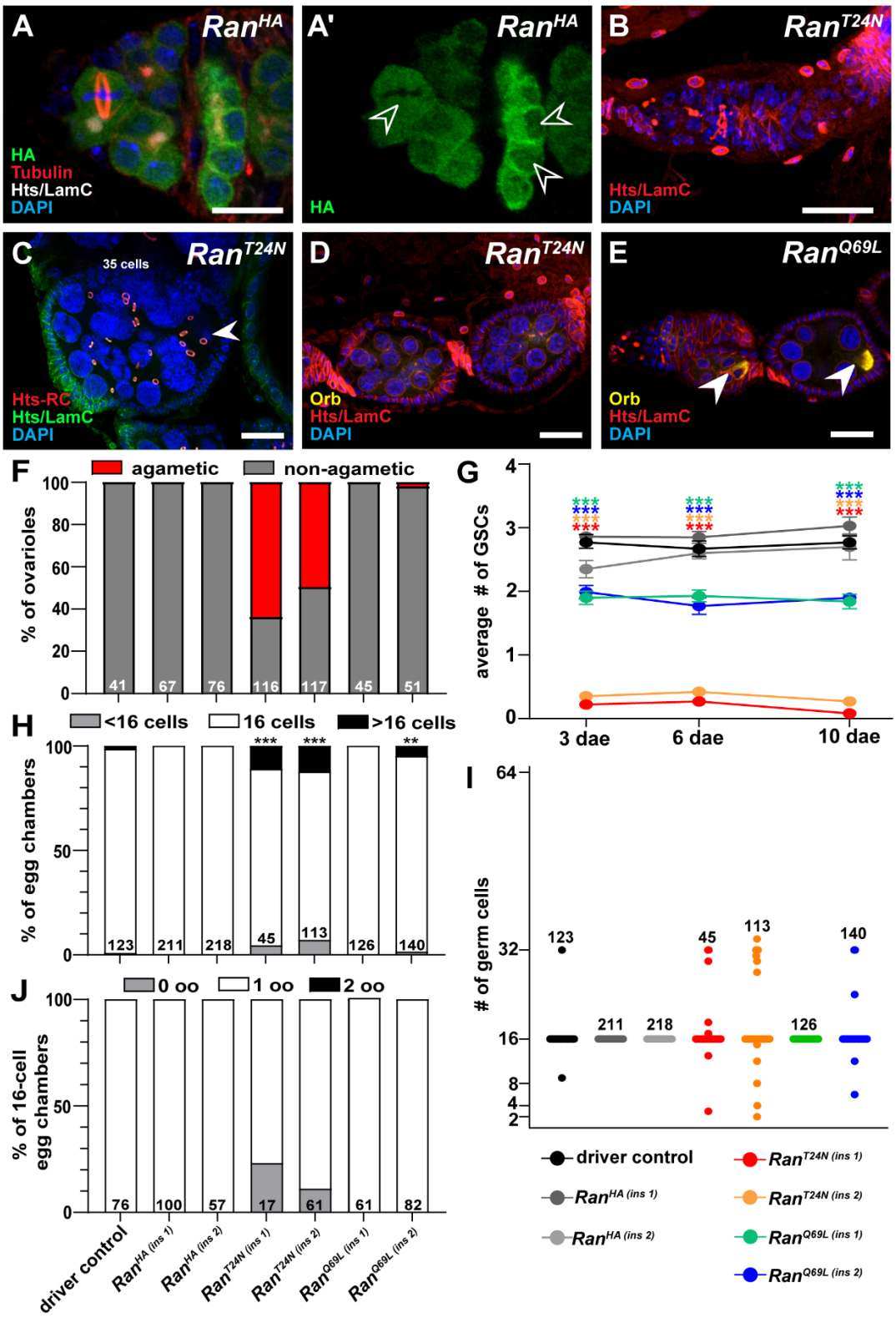

1000

1001 **Figure 4. Ran function in dividing germ cells requires Ran-GTP activity.**

1002 (A-A') Single z-plane image of a *nos-Gal4>Ran*^{HA} germarium labeled with anti-HA (green; Ran
1003 protein), anti-Tubulin (red; mitotic spindles), anti-Hts (white; fusomes and follicle cell
1004 membranes), anti-LamC (white; nuclear envelopes), and DAPI (blue; nuclei). The panel in A' is
1005 the HA-only image of the germarium at left. (B) Maximum intensity projection (10 µm subset) of
1006 a germarium from a *nos-Gal4>Ran*^{T24N} ovary immunostained with anti-Hts and anti-LamC (red),
1007 and DAPI (blue). (C) Maximum intensity projection (5 µm subset) representative *Ran*^{T24N}
1008 germarium stained with anti-Hts-RC (red; ring canals), anti-Hts and anti-LamC (green), and DAPI
1009 (blue). (D-E) Representative *Ran*^{T24N} (D, GDP-locked mutant) and *Ran*^{Q69L} (GTP-locked mutant)
1010 labeled with anti-Orb (yellow; oocyte), anti-Hts and anti-LamC (red), and DAPI (blue).
1011 Arrowheads indicate oocytes, as recognized by their condensed nuclei. (F) Frequencies of
1012 agametic (red) or non-agametic (grey) ovarioles in *nos-Gal4* control, *Ran* wild-type, and *Ran*
1013 dominant negative lines. Numbers in/above bars represent the total number of ovarioles analyzed.
1014 (G) Average number of GSCs at 3, 6, and 10 days after eclosion (dae). Dots indicate average
1015 number of GSCs at the point analyzed. More than 15 germaria per genotype at each timepoint were
1016 analyzed. (H) Frequencies of egg chambers containing less than 16 (grey), 16 (white), or more
1017 than 16 (black) germ cells per egg chamber in *nos-Gal4* control or *nos-Gal4* driving *Ran* wild-type
1018 and dominant negative transgenes at 6 dae. (I) Variation of the number of germ cells present per
1019 egg chamber. Numbers in/above bars represent the total number of egg chambers analyzed. (J)
1020 Frequencies of 16-cell egg chambers containing 0 (grey), 1 (white), or 2 (black) oocytes. In panels
1021 F, H, and J, the y-axis labels are identical. In panels H-J, numbers in/above bars represent the total
1022 number of egg chambers analyzed. Scale bars, 10 µm (A-A') and 20 µm (B-E). Error bars, mean
1023 ± SEM. $^{**}p < 0.01$; $^{***}p < 0.001$; Student's two-tailed T-test and Chi-squared tests.

1024

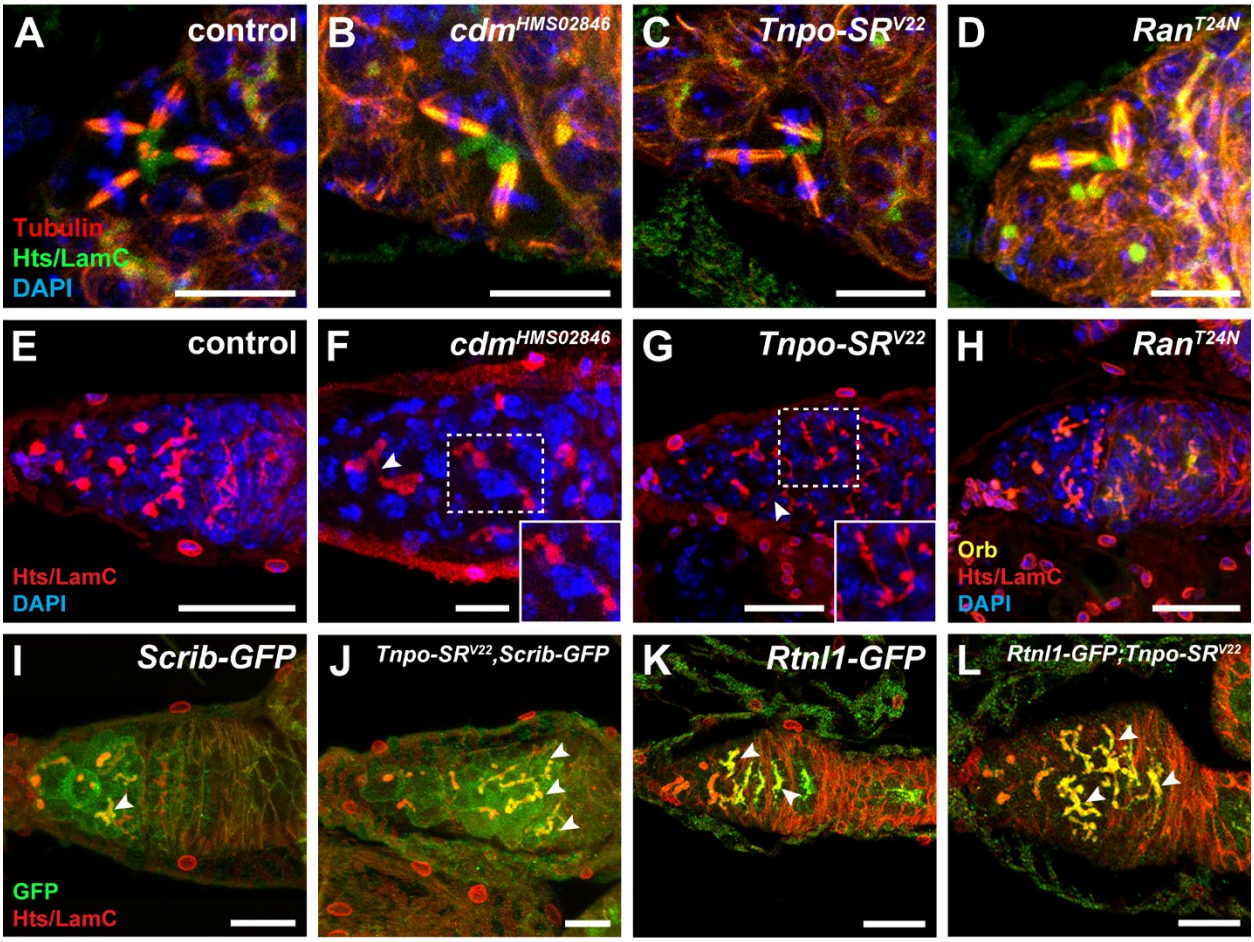

1025

1026 **Figure 5. *Tnpo-SR* and *cdm* are required for fusome integrity and maturation.**
1027 (A-D) Maximum intensity projections of representative driver control (A; 3 µm), *cdm*^{HMS02846} (B;
1028 3 µm), *Tnpo-SR*^{V22} (C; 7 µm), and *Ran*^{T24N} (D; 7 µm) mutant cysts labeled with anti-tubulin (red;
1029 mitotic spindles) anti-Hts (green; fusomes and follicle cell membranes, anti-LamC (green; nuclear
1030 envelope of cap cells), and DAPI (blue; nuclei). (E-H) Maximum intensity projections of
1031 representative driver control (E; 10 µm), *cdm*^{HMS02846} (F; 5 µm), *Tnpo-SR*^{V22} (G; 10 µm), and
1032 *Ran*^{T24N} (H; 5 µm) mutant germaria labeled with anti-Hts (red; fusomes and follicle cell
1033 membranes, anti-LamC (red; nuclear envelope of cap cells), and DAPI (blue; nuclei). Arrowheads
1034 indicate points of the fusome that are thinner than those seen in the control cysts. (I-J) Maximum
1035 intensity projections of representative *Scrib-GFP* control (I; 20 µm) and *Tnpo-SR*^{V22}*;Scrib-GFP*
1036 mutant (J; 20 µm) germaria labeled with anti-GFP (green), anti-Hts (red; fusomes and follicle cell
1037 membranes, and anti-LamC (red; nuclear envelope of cap cells). (K-L) Maximum intensity
1038 projections of representative *Rtnl1-GFP* control (K; 10 µm) and *Tnpo-SR*^{V22}*,Rtnl1-GFP* mutant

1039 (L; 10 μm) germaria labeled with anti-GFP (green), anti-Hts (red; fusomes and follicle cell
1040 membranes, and anti-LamC (red; nuclear envelope of cap cells). Arrowheads indicate highest level
1041 of expression of the Scrib (I-J) and Rtnl1 (K-L). Scale bar, 10 μm.
1042

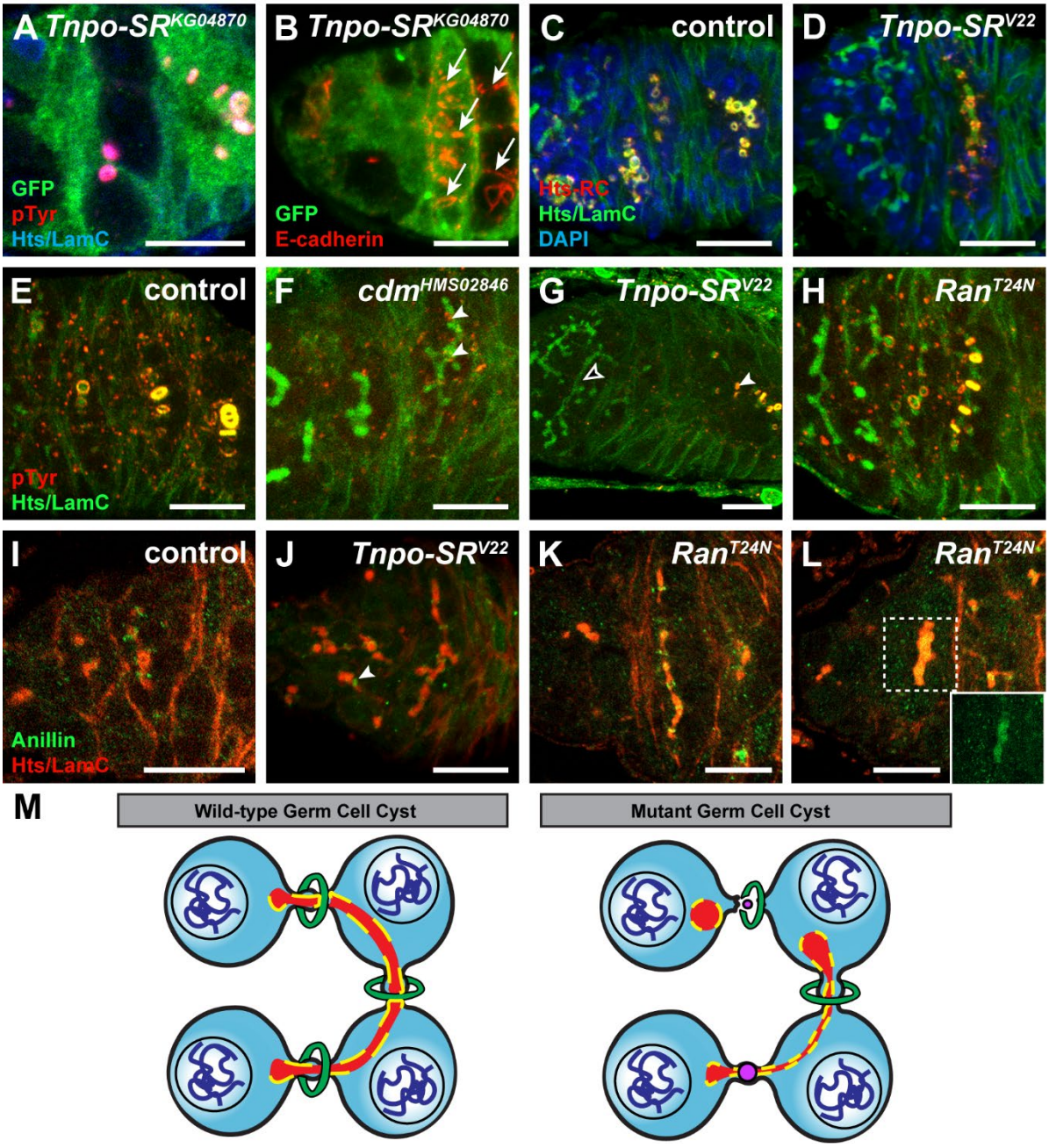

Figure 6. Depletion of *Tnpo-SR* and *cdm*, but not Ran-GTP, delays ring canal protein deposition and fails to suppress cytokinesis in dividing cysts.

(A) *Tnpo-SR*^{KG04870} mutant mosaic germarium labeled with anti-GFP (green; wild-type cells), anti-pTyrosine (pTyr, red; ring canals), anti-Hts (blue; fusomes and follicle cell membranes, and anti-LamC (blue; nuclear envelope of cap cells). (B) Maximum intensity projection of a *Tnpo-SR*^{KG04870} (5 µm subset) mutant mosaic germarium labeled with anti-GFP (green; wild-type cells) and anti-E-cadherin (red). Arrows indicate E-cadherin connections. (C-D) Representative control (C) and

1051 *Tnpo-SR*^{V22} (D) mutant germaria labeled with Hts-RC (red; ring canals), anti-Hts (green; fusomes
1052 and follicle cell membranes, anti-LamC (green; nuclear envelope of cap cells), and DAPI (blue;
1053 nuclei). (E-H) Maximum intensity projections (5 µm subsets) of representative driver control (E),
1054 *cdm*^{HMS02846} (F), *Tnpo-SR*^{V22} (G), and *Ran*^{T24N} (H) mutant cysts labeled with anti-pTyrosine (red;
1055 ring canals), anti-Hts (green; fusomes and follicle cell membranes), and anti-LamC (green; nuclear
1056 envelope of cap cells). Closed arrowheads indicate ring canals and open ring canals indicate a cyst
1057 that is lacking any remnants of ring canals. (I-L) Representative control (I), *Tnpo-SR*^{V22} mutant (J)
1058 and *Ran*^{T24N} mutant (K-L) germarium labeled with anti-anillin (green) anti-Hts (red; fusomes and
1059 follicle cell membranes), and anti-LamC (red; nuclear envelope of cap cells). Arrowheads indicate
1060 closed ring canals. Scale bar, 10 µm. (M) Summary of fusome and ring canal phenotypes in *Tnpo-*
1061 *SR*- and *cdm*-depleted germ cell cysts.
1062

1063

1064

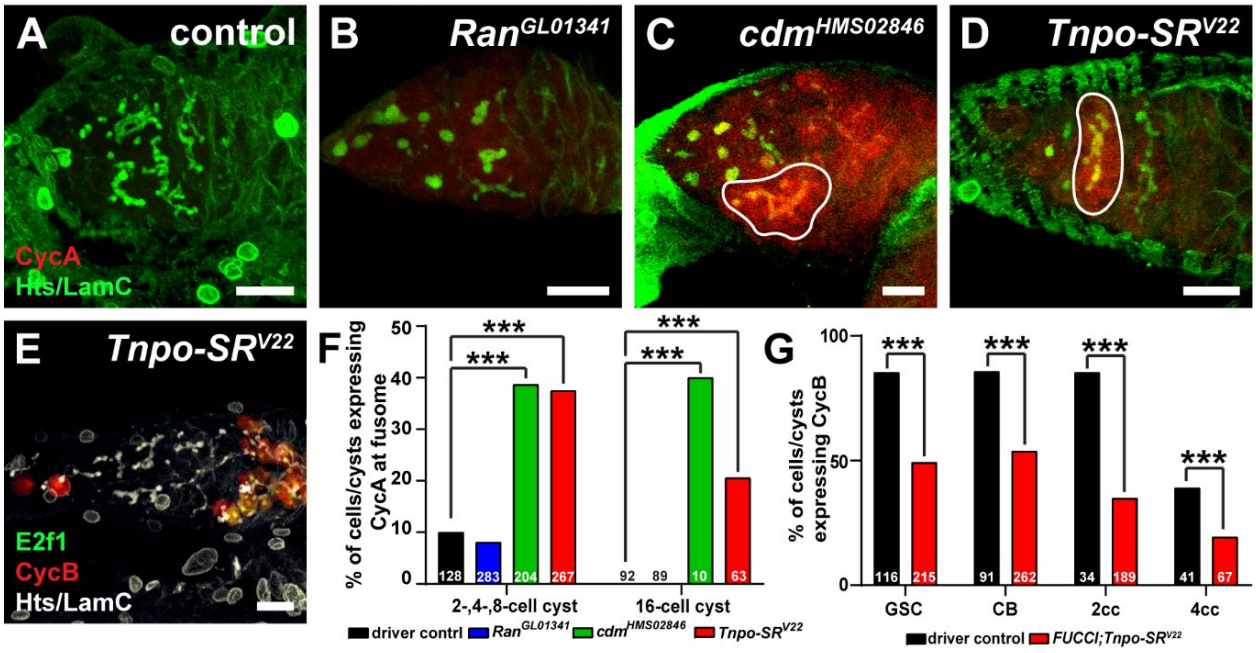

Figure 7. CycA is ectopically expressed in c*dm* and *Tnpo-SR* cysts.

(A-D) Maximum intensity projections (10 µm subsets) of representative driver control (A), *Ran*^{GL01341} (B), *cdm*^{HMS02846} (C), and *Tnpo-SR*^{V22} (D) mutant germaria labeled with anti-CycA (red), anti-Hts (green; fusomes and follicle cell membranes, and anti-LamC (green; nuclear envelope of cap cells). (E) Maximum intensity projection of *nos-Gal4>FUCCI;Tnpo-SR*^{V22} labeled with anti-GFP (green; E2f1), anti-dsRed (red; CycB), and anti-Hts (white; fusomes and follicle cell membranes, and anti-LamC (white; nuclear envelope of cap cells). Scale bar, 10 µm. (F) Percentage of cells/cysts containing fusome-localized CycA. (G) Percentage of cells/cysts containing *RFP::CycB* in *nos-Gal4* controls and *Tnpo-SR*^{V22} knockdown germaria. The number of cells/cysts analyzed is shown above bars. ***$p < 0.001$, Student's Chi-squared test.

1077 **SUPPLEMENTAL DATA**

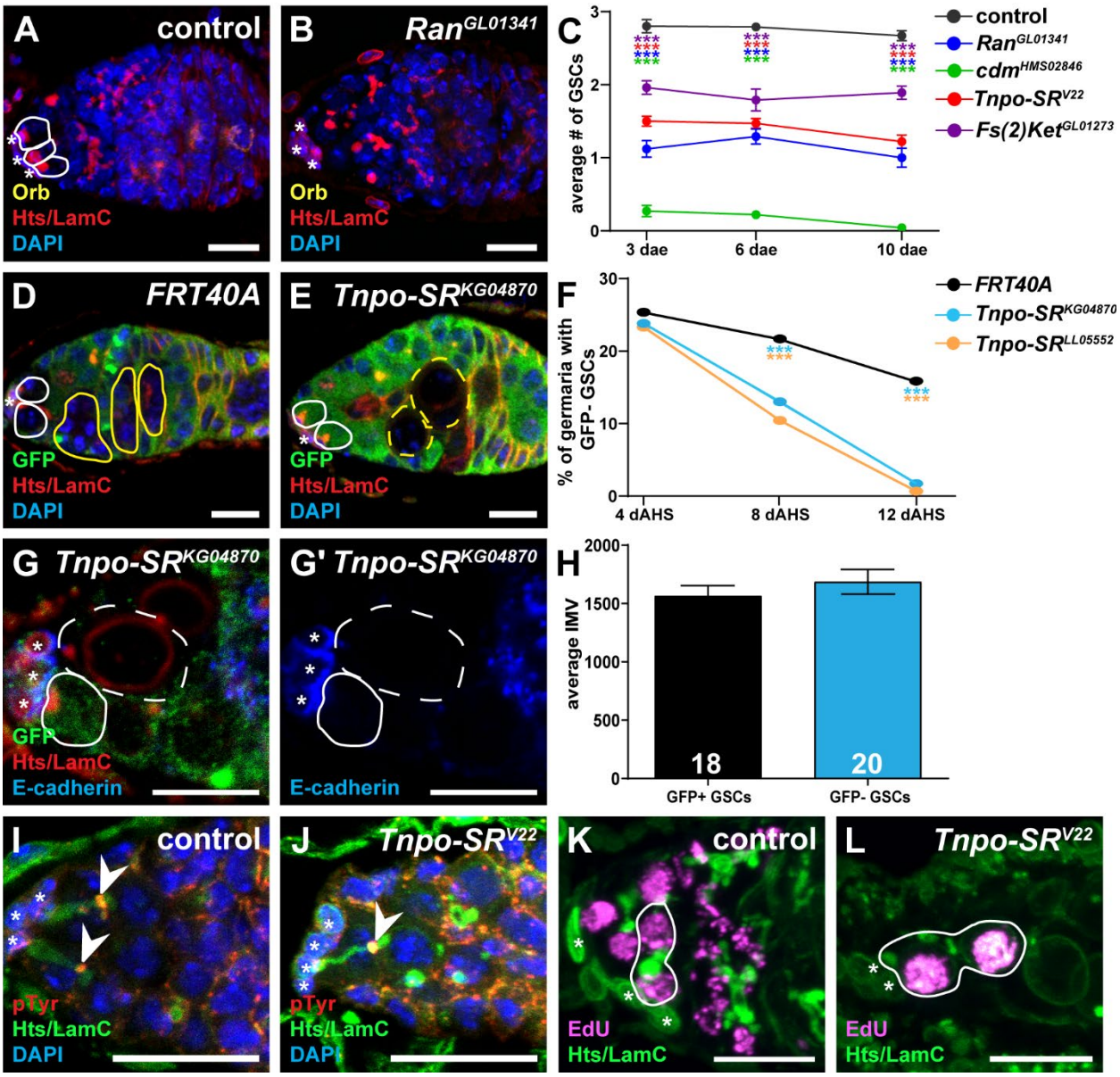

1078

1079 **Supp. Figure 1. Ran and β-importins are necessary for GSC maintenance.**

1080 (A-B) Max intensity projections (10 µm subset) of *nos-Gal4* control (A) and *nos-Gal4>UAS-*
1081 *Ran*^{GL01341} (B) germaria labeled with anti-orb (yellow; oocyte), anti-Hts (red; fusomes and follicle
1082 cell membranes, anti-LamC (red; nuclear envelope of cap cells) and DAPI (blue; nuclei). Solid
1083 white lines demarcate GSCs present in the germarium, asterisks indicate cap cells. (C) Average
1084 number of GSCs per germarium in *nos-Gal4* control or *nos-Gal4>UAS-Ran/importin RNAi* ovaries
1085 at 3, 6, and 10 days after eclosion (dae). At least 30 germaria were analyzed at each timepoint. (D-

1086 E) Single z-plane confocal micrographs of *FRT40A* control (D) and *Tnpo-SR*^{KG04870} *FRT40A*
1087 mutant (E) mosaic germaria at 8 days after clone induction labeled with anti-GFP (green; wild-
1088 type cells), anti-Hts (red; fusomes and follicle cell membranes), anti-LamC (red; nuclear
1089 envelopes) and DAPI (blue; nuclei). Lines demarcate wild-type (solid) or mutant (dashed) GSCs
1090 (white) and cystoblast/cysts (yellow). (F) Percentage of total germaria analyzed with a GFP-
1091 negative GSC at 4, 8, and 12 days after clone induction. At least 145 germaria were analyzed. (G-
1092 G') *Tnpo-SR*^{KG04870} mutant mosaic germaria at 8 days after clone induction labeled with anti-GFP
1093 (green; wild-type cells), anti-Hts and anti-LamC (red), and anti-E-cadherin (blue). Lines demarcate
1094 wild-type (solid) or mutant (dashed) GSCs. Image in G' is the E-cadherin channel only of the
1095 image in G. (H) Average intensity mean value (IMV) of E-cadherin at the GSC-cap cell junction
1096 of GFP-positive (wild-type) or GFP-negative (*Tnpo-SR*^{KG04870} mutant) GSCs at 8 days after clone
1097 induction. Numbers in the bars represent the total number of GSCs analyzed. (I-J) Max intensity
1098 projections (2 µm subset) of *nos-Gal4* control (I) and *nos-Gal4>Tnpo-SR*^{V22} (J) GSC/CB pairs
1099 labeled with anti-pTyrosine (red; ring canals), anti-Hts and anti-LamC (green), and DAPI (blue).
1100 Arrowheads indicate pTyr+ plug that forms between the GSC/CB pair prior to abscission. (K-L)
1101 Max intensity projections (10 µm subset) of *nos-Gal4* control (K) and *nos-Gal4>Tnpo-SR*^{V22} (L)
1102 GSC/CB pairs labeled with anti-Edu (magenta; S-phase marker), anti-Hts and anti-LamC (green).
1103 Scale bars, 10 µm. Error bars, mean ± SEM. ***$p < 0.001$; Student's two-tailed T-test.

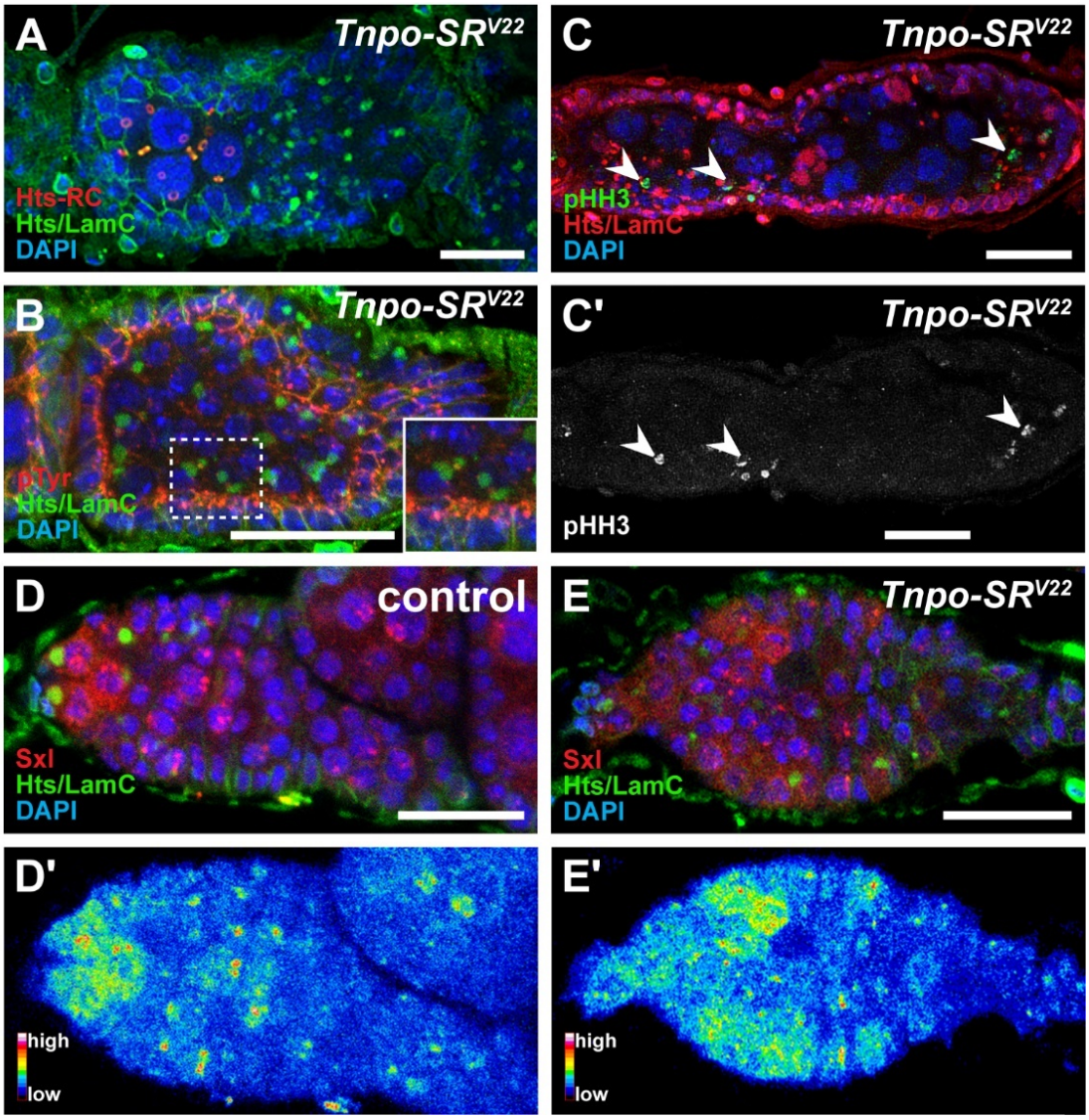

Supp. Figure 2. *Tnpo-SR* germline tumors are primarily composed of mitotically-dividing undifferentiated germ cells.

(A) Maximum intensity projection (20 µm subset) of a *nos-Gal4>Tnpo-SR*^{V22} egg chamber labeled with anti-Hts-RC (red; ring canals), anti-Hts (green; fusomes and follicle cell membranes), anti-LamC (green; nuclear envelopes), and DAPI (blue; nuclei). (B) Maximum intensity projection (20 µm subset) of a *nos-Gal4>Tnpo-SR*^{V22} egg chamber labeled with anti-pTyr (red; ring canals), anti-Hts and anti-LamC (green), and DAPI (blue). (C) Maximum intensity projection (10 µm subset) of a *nos-Gal4>Tnpo-SR*^{V22} egg chamber labeled with anti-pHH3 (green; M-phase marker), anti-Hts and anti-LamC (red), and DAPI (blue). Panel in C' depicts pHH3 channel only. Arrowheads indicate pHH3-positive cells within the germline tumor. (D-E) Representative control (D) and *nos-*

1115 *Gal4>Tnpo-SR*^{V22} (E) germaria labeled with anti-Sxl (red), anti-Hts and anti-LamC (green), and
1116 DAPI (blue). Panels D' and E' show heat maps corresponding to panels D and E, where cool colors
1117 are low expression and warm colors are high expression. Scale bars, 20 µm.
1118

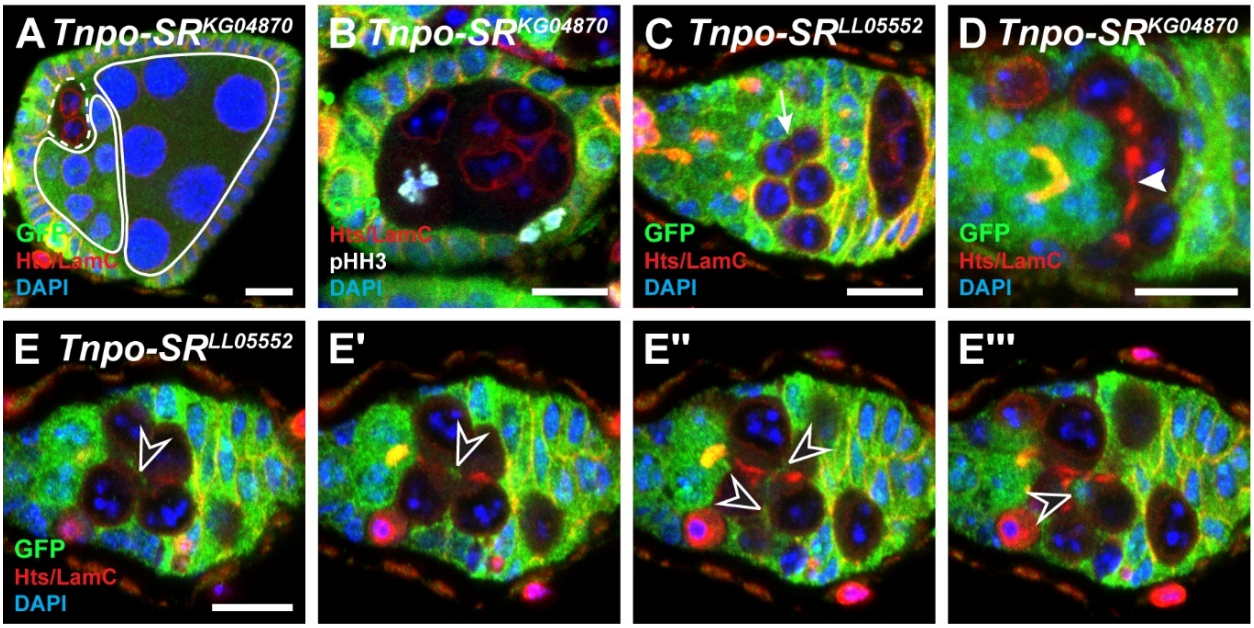

Supp. Figure 3. *Tnpo-SR* mutants fail to maintain cyst connectivity and some cells are ectopically mitotically active.

(A) *Tnpo-SR*^{KG04870} mutant egg chamber labeled with anti-GFP (green; wild-type cells), anti-Hts (red; fusomes and follicle cell membranes), anti-LamC (red; nuclear envelopes), and DAPI (blue; nuclei). White lines indicate wild-type cysts (solid) and mutant cysts (dashed). (B) *Tnpo-SR*^{KG04870} mutant egg chamber labeled with anti-GFP (green; wild-type cells), anti-pHH3 (white; M-phase), anti-Hts (red; fusomes and follicle cell membranes), anti-LamC (red; nuclear envelopes), and DAPI (blue; nuclei). (C-E''') *Tnpo-SR*^{LL05552} (C and E-E''') and *Tnpo-SR*^{KG04870} (D) mutant germaria labeled with anti-GFP (green; wild-type cells), anti-Hts (red; fusomes and follicle cell membranes), anti-LamC (red; nuclear envelopes), and DAPI (blue; nuclei). Closed arrowhead represents thin thread of fusome material and open arrowheads follow the GFP+ follicle cell projections invaginating the mutant cysts. (D) is a 2 µm subset maximum intensity projection. Scale bar, 10 µm.

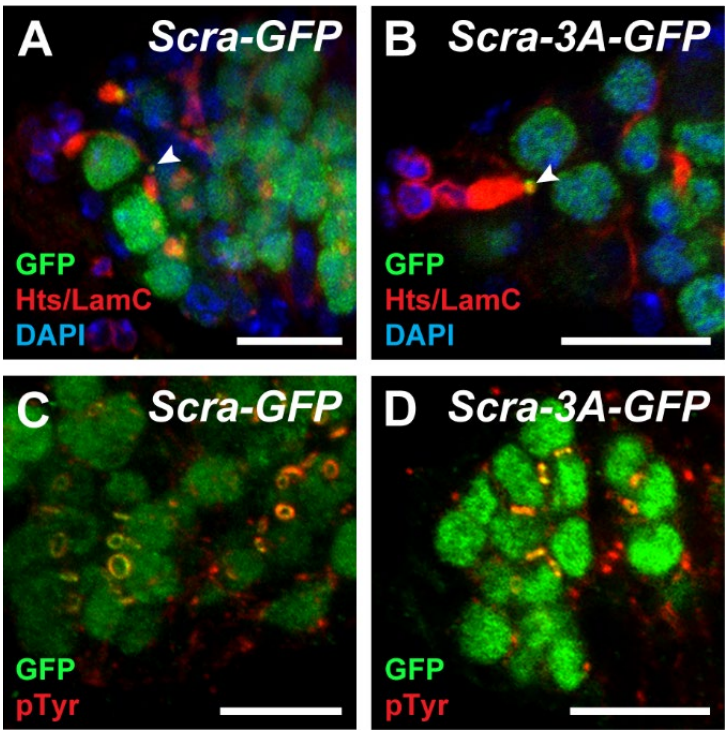

1134

1135 **Supp. Figure 4. An Anillin-NLS mutant is not efficient in disrupting anillin localization to**
1136 **nuclei and ring canals.**

1137 (A-D) Representative controls of *UAS-Scra-GFP* (A and C) and NLS mutated *UAS-Scra-3A-GFP*
1138 mutant (B and D) germaria labeled with anti-GFP (green), anti-Hts (red; fusomes and follicle cell
1139 membranes), and anti-LamC (red; nuclear envelope of cap cells), and DAPI (blue nuclei) (A-B) or
1140 anti-pTyrosine (red; ring canals) (C-D). Arrowheads indicate closed ring canals. Scale bar, 10 µm.

1141

1142 **Supp. Table S1.** Fly stocks and immunofluorescence reagents used in this study.

Reagent	Source	Reference
nos-GAL4::VP16-nos.UTR	D. Drummond-Barbosa	(Rørth, 1998; Van Doren et al., 1998)
w; nosGal4::VP16, UASp-tubGFP*	BLM #7253	(Grieder et al., 2000)
Tnpo-SR^{V22}	Ables Lab	this study
y^{1}*v*^{1}*; P{y[+t7.7] v[+t1.8]=TRiP.GL01483}attP2*	BLM #43142	(Perkins et al., 2015)
y^{1}*sc***v*^{1}*sev*^{21}*; P{y[+t7.7] v[+t1.8]=TRiP.GL01341}attP40*	BLM #42482	(Perkins et al., 2015)
y^{1}*sc***v*^{1}*sev*^{21}*; P{y[+t7.7] v[+t1.8]=TRiP.HMS02846}attP2*	BLM #44551	(Perkins et al., 2015)
y^{1}*v*^{1}*; P{y[+t7.7] v[+t1.8]=TRiP.HMS00020}attP2*	BLM #33626	(Perkins et al., 2015)
y^{1}*sc***v*^{1}*sev*^{21}*; P{y[+t7.7] v[+t1.8]=TRiP.HMS01408}attP2*	BLM #34998	(Perkins et al., 2015)
y^{1}*sc***v*^{1}*sev*^{21}*; P{y[+t7.7] v[+t1.8]=TRiP.HMS00991}attP2*	BLM #34021	(Perkins et al., 2015)
y^{1}*v*^{1}*; P{y[+t7.7] v[+t1.8]=TRiP.GL01273}attP2*	BLM #41845	(Perkins et al., 2015)
y^{1}*sc***v1; P{y[+t7.7] v[+t1.8]=TRiP.HMS02968}attP2*	BLM #50732	(Perkins et al., 2015)
y^{1}*sc***v*^{1}*sev*^{21}*; P{y[+t7.7] v[+t1.8]=TRiP.GL00435}attP40*	BLM #35598	(Perkins et al., 2015)
y^{1}*sc***v*^{1}*sev*^{21}*; P{y[+t7.7] v[+t1.8]=TRiP.HMC03738}attP40*	BLM #55142	(Perkins et al., 2015)
y^{1}*v*^{1}*; P{y[+t7.7] v[+t1.8]=TRiP.HMJ22418}attP40/CyO*	BLM #58311	(Perkins et al., 2015)

$y^1sc^*v^1sev^{21}$; P{y[+t7.7] v[+t1.8]=TRiP.HMC04414}attP40	BLM #56974	(Perkins et al., 2015)
y^1v^1; P{y[+t7.7] v[+t1.8]=TRiP.HMJ23009}attP40	BLM #61230	(Perkins et al., 2015)
hsFLP; FRT40A, UbiGFP / CyO	D. Drummond-Barbosa	(Ables et al., 2016)
FRT40A / CyO	D. Drummond-Barbosa	(Ables et al., 2016)
$y^{d2}w^{1118}$ P{ry[+t7.2]=ey-FLP.N}2 P{ry[+t7.2]=GMR-lacZ.C(38.1)}TPN1; P{y[+mDint2] w[BR.E.BR]=SUPor-P}Trn-SR[KG04870] P{ry[+t7.2]=neoFRT}40A / CyO, y[+]	Kyoto #111581	(Bellen et al., 2004; Chen et al., 2005)
y^*w^*; PBac{SAstopDsRed}LL05552 P{ry[+t7.2]=neoFRT}40A P{w[+mW.hs]=FRT(w[hs])}G13 cn^1bw^1 / CyO, S^*bw^1	Kyoto #141628	(Schuldiner et al., 2008)
w;P{UASp:Ran^{HA}}1.19/SM6	K. McKim	(Cesario and McKim, 2011)
w;P{UASp:Ran^{HA}}10-A/TM3	K. McKim	(Cesario and McKim, 2011)
w;P{UASp:Ran^{T24NHA}}18.3/TM3	K. McKim	(Cesario and McKim, 2011)
w;P{UASp:Ran^{T24NHA}}25.1/TM3	K. McKim	(Cesario and McKim, 2011)
w;P{UASp:Ran^{Q69LHA}}7.1/TM3	K. McKim	(Cesario and McKim, 2011)
w;P{UASp:ran^{Q69LHA}}61.2/TM3	K. McKim	(Cesario and McKim, 2011)
w[1118]; P{UASp-GFP.E2f.1-230}26 P{UASp-mRFP1.NLS.CycB.1-266}4/CyO,P{en1}wg[en11];MKRS/TM6B, Tb1	BLM #55110	(Zielke et al., 2014)
Rtnl1-GFP	B. Riggs, K. Röper	(Röper, 2007)
$scrib^{CA07683}$	L. Cooley, M. Buszczak	(Buszczak et al., 2007)

w; P{w[+mC]=UASp-GFP-scra}3*	BLM #51348	(Silverman-Gavrila et al., 2008)
w; wg^{Sp-1}/CyO; P{w[+mC]=UASp-GFP-3A-scra}3*	BLM #51347	(Silverman-Gavrila et al., 2008)

1143

1144

1145